

Swarthmore College

Works

Senior Theses, Projects, and Awards


Student Scholarship

Spring 2023

Using *Caulobacter crescentus* as a Model to Probe the Environmental Reactivity of Silver Nanoparticles

Madeline M. Farber , '23

Follow this and additional works at: <https://works.swarthmore.edu/theses>

 Part of the [Chemistry Commons](#)

Recommended Citation

Farber, Madeline M. , '23, "Using *Caulobacter crescentus* as a Model to Probe the Environmental Reactivity of Silver Nanoparticles" (2023). *Senior Theses, Projects, and Awards*. 263.

<https://works.swarthmore.edu/theses/263>



This work is licensed under a [Creative Commons Attribution-Share Alike 4.0 International License](#).

This work is brought to you for free by Swarthmore College Libraries' Works. It has been accepted for inclusion in Senior Theses, Projects, and Awards by an authorized administrator of Works. For more information, please contact myworks@swarthmore.edu.

Using *Caulobacter crescentus* as a Model to Probe the Environmental Reactivity of Silver Nanoparticles

Presented as a Senior Honors Thesis in Chemistry

Madeline M. Farber

May 18th, 2023

Department of Chemistry and Biochemistry, Swarthmore College, Swarthmore PA

Advisor: Kathryn R. Riley

Table of Contents

List of Common Abbreviations	iv
List of Figures and Tables.....	v
Abstract.....	1
Chapter 1: Introduction.....	2
1.1: Silver Nanoparticles and Their Environmental Impact	3
1.2: Model Systems to Investigate Nanoparticle Toxicity	7
1.2.1: <i>Caulobacter crescentus</i> Background and Relevance.....	8
1.2.2: Modeling the Cell Plasma Membrane	10
1.3: The Eco-Corona.....	13
1.4: Proposed Work	15
Chapter 2: Materials and Methods	17
2.1: Chemicals.....	17
2.2: Culturing <i>Caulobacter crescentus</i>	18
2.3: <i>In Vivo</i> Toxicity Studies	19
2.4: Eco-Corona Formation	21
2.5: Liposome Preparation	22
2.6: Size and Surface Potential Characterization by DLS	23
2.6.1: Liposome Characterization	24
2.6.2: AgNP Characterization	24
2.7: UV-Vis Characterization of AgNPs	24
2.8: Probing Time-dependent Liposome Size Changes with DLS	24
2.9: Probing Time-dependent Membrane Fluidity Changes with Fluorescence Anisotropy.....	25
Chapter 3: AgNP Toxicity to <i>C. crescentus</i> is Modulated by the Presence of an Eco- Corona.....	27
3.1: Characterization of AgNPs and SM-AgNPs with DLS and UV-Vis.....	27
3.2: AgNPs and SM-AgNPs Induce Distinct Effects on <i>C. crescentus</i> Growth....	31
Chapter 4: Development of a Model Membrane System Based on <i>C. crescentus</i> to Evaluate AgNP Reactivity	34
4.1: Modeling the <i>C. crescentus</i> Membrane with Large Unilamellar Vesicles	34

4.2: Optimization of Fluorescence Anisotropy to Measure Changes in Membrane Fluidity	35
Chapter 5: Quantifying Time-Dependent Changes in the <i>C. crescentus</i> Phospholipid Bilayer Induced by AgNPs	39
5.1: The Eco-Corona Modulates AgNP Adhesion to the <i>C. crescentus</i> Bilayer ...	39
5.2: AgNP Adhesion to the <i>C. crescentus</i> Bilayer Increases Membrane Rigidity	43
Chapter 6: Conclusions and Future Directions	46
Acknowledgments.....	52
Appendix.....	53
References.....	55

List of Common Abbreviations

AgNP – Silver nanoparticle
CL – Cardiolipin
DLS – Dynamic light scattering
DPH – Diphenylhexatriene
ENM – Engineered nanomaterial
GUV – Giant unilamellar vesicle
LSPR – Localized surface plasmon resonance
LUV – Large unilamellar vesicle
MLV – Multilamellar vesicle
NOM – Natural organic matter
OD – Optical density
PC – Phosphatidylcholine
PG – Phosphatidylglycerol
PDI – Polydispersity index
QCM-D – Quartz crystal microbalance with dissipation
ROS – Reactive oxygen species
SLB – Supported lipid bilayer
SM – Spent medium
SUV – Small unilamellar vesicle
PYE – Peptone-yeast extract
 ζ – Zeta potential

List of Figures and Tables

Figure 1. Schematic of the dimorphous life cycle of <i>C. crescentus</i> including stalked and swarmer cells.	9
Figure 2. Schematic of the extruder apparatus used in liposome preparation..	22
Figure 3. Representative UV-Vis spectra of AgNPs and SM-AgNPs prior to incubation at 30 °C.	30
Figure 4. OD ₆₀₀ growth curves of <i>C. crescentus</i> (control), in the presence of 2 mg L ⁻¹ AgNPs, and in the presence of 2 mg L ⁻¹ SM-AgNPs.	33
Figure 5. Schematic of the 9:1 PGCL large unilamellar vesicle.....	34
Figure 6. Excitation and emission spectra of 10 µM DPH in acetone.	36
Figure 7. Optimization of DPH concentration and embedding method.	38
Figure 8. PGCL liposome hydrodynamic diameters over 24 hours at 30 °C.	40
Figure 9. DLS histograms showing the averaged size distributions of PGCL liposomes (control) over 24 hours at 30 °C and the changes induced by (SM-)AgNPs.....	42
Figure 10. Anisotropy, $\langle r \rangle$, of DPH-embedded PGCL liposomes over 24 hours at 30 °C and the changes induced by (SM-) AgNPs.....	44
Figure 11. Proposed mechanism of interaction of AgNPs with phospholipid bilayers. ..	48
Table 1. Experimental AgNP hydrodynamic diameters and zeta potentials, obtained through DLS.....	28
Table 2. Fit Parameters of Boltzmann sigmoidal distributions for the growth of <i>Caulobacter crescentus</i> in the presence of (SM-) AgNPs	33

Abstract

Silver nanoparticles (AgNPs) are an increasingly common environmental pollutant with antimicrobial and antibacterial properties. The elucidation of their interaction with cellular membranes and subsequent mechanisms of toxicity are critical areas of research that need to be better understood in order to manage potential adverse environmental effects. This work investigates the interaction of AgNPs with large unilamellar vesicles (LUVs) as a model membrane system. Similar studies conducted by others in this field have largely been conducted with uncoated AgNPs, ignoring the effect of environmental conditions on the formation of an eco-corona on AgNPs. Thus, in this study, the spent medium (SM) of a relevant environmental bacterium, *Caulobacter crescentus*, was used to form a complex eco-corona. We hypothesized that the eco-corona would mediate the *in vivo* reactivity of AgNPs, specifically through distinct interactions at the cell membrane. The differential reactivity of AgNPs and SM-AgNPs is shown through an *in vivo* toxicity study using *C. crescentus*. Model membranes were analyzed using dynamic light scattering (DLS), in which AgNP and LUV size and charge are characterized, and fluorescence anisotropy, where changes to LUV membrane fluidity and dynamics are interrogated. Results of the *in vivo* study are presented in tandem with model membrane studies in order to correlate toxicity effects seen *in vivo* with potential mechanisms of reactivity at the cell membrane.

Chapter 1: Introduction

Industrial, commercial, and medicinal use of engineered nanomaterials (ENMs) has increased exponentially in the last decade due to their easily tunable size and unique properties compared to their bulk counterparts. In particular, silver nanoparticle (AgNP) usage has grown from a global market of less than 300 tons in 2010 to a projected 800 tons in 2025.¹ Enthusiasm regarding the antimicrobial and antibacterial nature of AgNPs has led to their incorporation into industrial, commercial, and medical products. For example, a wide assortment of products including health and fitness equipment, cosmetics, industrial foams, water filters, and paints now contain these novel nanomaterials.² The antibacterial nature of AgNPs has led to a rapid increase in their availability in the market, greatly improving quality of life for the consumer, however, this must be met with caution due to their toxicity and potential negative environmental implications.³ As AgNPs gain prevalence, their release into the environment and interaction with living organisms is inevitable. The biocidal nature of AgNPs may have potentially severe adverse effects on the environment and its inhabitants.

Despite the pervasiveness of AgNPs in the environment and their potential cytotoxic effects, the specific mechanisms of their interaction with organisms are poorly understood. Due to their high surface area to volume ratio, AgNPs easily undergo several transformations in the environment that subsequently affect their properties, transport, and ultimately, their fate. These include aggregation,^{4,5} dissolution,⁶⁻⁸ sulfidation,⁹ and adsorption of macromolecules such as proteins^{10,11} and natural organic matter.^{12,13} The downhill effect of these transformations on AgNP toxicity and antibacterial activity has been poorly characterized. Of particular importance, AgNPs readily form an eco-corona

upon introduction into a natural environment. Eco-coronas are complex mixtures of biomolecules, natural organic matter (NOM), environmental contaminants, and inorganic ions that adsorb onto the surface of the nanoparticle, leading to changes in their surface characteristics, properties, and interactions.¹⁴ Although this coating of adsorbates likely modulates the toxicity mechanisms of AgNPs,^{10,15} eco-coronas are still poorly understood. This work aims to bridge two current areas of nanoparticle research: the formation of an eco-corona in natural conditions and the subsequent interactions of coronated nanoparticles with living organisms. A suite of analytical methods was developed to characterize the interactions at the nano-bio interface and to begin to understand the toxicity mechanisms of AgNPs as well as the potential role of eco-coronas in modulating toxicity.

1.1: Silver Nanoparticles and Their Environmental Impact

An ENM is defined as any material with at least one dimension in the nanoscale, from 1-100 nm. ENMs vary widely in composition, with the current market including non-metallic inorganic nanoparticles, like TiO₂ nanoparticles which are commonly found in sunscreens;¹⁶ metals and metal alloys, including the AgNPs discussed in this work; carbon-based nanomaterials, such as fullerenes used as therapeutic agents in the medical field;¹⁷ nanopolymers and dendrimers; and quantum dots, like CdSe nanoparticles often used in sensing and imaging.^{2,18} These materials also come in a wide variety of shapes and sizes that further determine their distinctive characteristics. The unique antibacterial and antimicrobial activity of AgNPs have led to their applications in a wide assortment of industrial, commercial, and medical products that capitalize on these characteristics, leading to a huge increase in their availability on the global market.

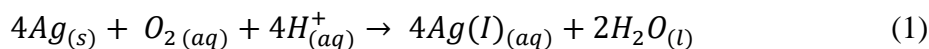
The antibacterial properties of AgNPs have been shown to greatly improve the quality of life, human and otherwise, with novel applications ranging from improving the growth of plants,¹⁹ preserving cosmetic and beauty products,²⁰ filtering dangerous microbes from drinking water,²¹ sterilizing wound dressings,^{22–25} and reducing odor and bacterial growth in exercise equipment.²⁶ However, it would be simplistic to assume that the antibacterial nature of AgNPs is universally good. While some bacteria are pathogenic and dangerous, like those causing infections in surgery patients, AgNPs do not distinguish between these “bad” bacteria and others which are necessary for environmental health and ecosystem sustainability. While this non-specific toxicity makes AgNPs useful for many different applications, it also raises concern for their environmental impact. Not only have bacteria led to substantial advances in human health through discoveries in the fields of biotechnology, agriculture, and medicine, but also their very existence is critical to the survival of the planet.²⁷ These “good” bacteria can be found everywhere there is life, most prominently in the gut microbiome,²⁸ in natural water sources as essential components of the ecosystem,^{29–31} on human skin as a natural support for the immune system,³² and in soils providing essential nutrients for plant growth.³³ While the antibacterial nature of AgNPs is often exploited for consumer uses, the potential harmful effects on “good” bacteria need further study in order to regulate this rapidly growing market.

After use in industrial, commercial, and medical products, AgNPs can be released into the environment through washing and improper disposal where they can potentially have adverse effects on these so-called “good” bacteria. Upon introduction to the environment, AgNPs can undergo a variety of dynamic transformations, including

aggregation and dissolution that effect their fate and transport. AgNPs also rapidly adsorb biomolecules to their highly reactive surfaces (see Section 1.3 for more details). While other transformations are possible, this discussion will be limited to the three mentioned above.

Aggregation kinetics of AgNPs can be explained reasonably using the Derjaguin-Landau-Verwey-Overbeek (DLVO) theory to describe stability of colloids. Aggregation of AgNPs is largely based on electrostatic forces in solution, with the most critical factors that influence aggregation being solution chemistry and coatings present on the nanoparticle. The presence of a coating on AgNPs, such as a negatively charged citrate layer, serves to stabilize the particles in solution through an electrostatic barrier, preventing aggregation. An increase in ionic strength in solution can shield this charge repulsion between particles, leading to greater aggregation.^{6,34} In their interactions with bacterial cells, AgNPs are observed to accumulate and form aggregates at the cell plasma membrane, leading to a loss of membrane integrity and eventual cell death.³⁵ This has been readily observed in several species of bacteria, including *Escherichia coli*,³⁶ *Staphylococcus aureus*,³⁷ and several serovars of *Salmonella*.³⁸

Dissolution also greatly impacts the toxicity of AgNPs on bacterial life. When silver atoms at the surface of the nanomaterial encounter an oxidizing species in solution, ionic silver ($\text{Ag(I)}_{(aq)}$) is produced via oxidative dissolution according to:



$\text{Ag(I)}_{(aq)}$ can deactivate several critical biological systems, for example DNA and cell replication, due to its high affinity for certain functional groups commonly found in cells.³⁵ Several factors affect the dissolution rate of AgNPs, including surface coatings of

the nanoparticle,³⁹ adsorbates,^{40–44} ionic strength and pH of the solution,^{45–47} and particle size.^{44,45,48,49} Smaller particles are known to dissolve faster than larger particles, showing the importance of the accessibility of the surface area to interact with dissolved oxygen species. While bulk silver can also dissolve into $\text{Ag(I)}_{(aq)}$, its dissolution rate is much slower than nanosilver. Additionally, it has been suggested that the accumulation of AgNPs at the cell plasma membrane may allow generation of cytotoxic $\text{Ag(I)}_{(aq)}$ in much closer proximity to the cell interface than bulk silver could achieve.³⁶ $\text{Ag(I)}_{(aq)}$ has been shown to be bactericidal in several species of bacteria, including *Escherichia coli* and *Staphylococcus aureus* through disruptions in the cell plasma membrane as well as to biological functions of the cell.⁵⁰

AgNP antibacterial toxicity could also be due to the enhanced generation of reactive oxygen species (ROS) in cells, subsequently leading to high levels of oxidative stress. AgNPs enhance generation of ROS in cells in a size-dependent manner, with smaller particles having a greater ability to produce the free radical species because of their increased surface area to volume ratio.⁵¹ ROS can also trigger further cell disruptions, including DNA modification and inhibition of cell reproduction.⁵² The exact mechanism of how AgNPs and $\text{Ag(I)}_{(aq)}$ are toxic to bacterial life has not yet been fully understood. Several potential mechanisms have been suggested that highlight the roles of the neutral silver core and its aggregation near the cell plasma membrane, the dissolution of AgNPs into $\text{Ag(I)}_{(aq)}$ that can also disrupt the membrane, and the generation of ROS by the nanoparticles. Likely, no one mechanism is responsible for AgNP toxicity, and all three play a role in contributing to toxicity. Whether due to the combination of these three mechanisms: intracellular particle accumulation, ROS generation, and dissolution, or a

mechanical interaction with the bilayer, AgNPs show unique reactivities compared to $\text{Ag(I)}_{(aq)}$ alone.^{53–56}

1.2: Model Systems to Investigate Nanoparticle Toxicity

Regarding cytotoxic interactions between AgNPs and cells, recent literature has highlighted the crucial role of the cell plasma membrane as a defensive mechanism and a first point of contact for the nanoparticles. The cell plasma membrane is a lipid bilayer that separates the cytoplasm of a cell from the extracellular matrix. This membrane is a complex fluid bilayer and often contains transmembrane proteins, ion channels, and other important macromolecules to regulate cell function and defense.^{57,58} Beyond the disruption of biological processes induced by $\text{Ag(I)}_{(aq)}$ and ROS, AgNPs can also cause disruption directly to the cell plasma membrane.⁵⁹ AgNPs have been observed to accumulate at the cell plasma membrane as aggregates,³⁵ form “pits” in the membrane that disrupt the structure and viability of cells,³⁶ and disrupt the membrane potential or block critical ion channels.⁶⁰ In developing a complete understanding of the mechanism of toxicity of AgNPs on cells, studying the nano-bio interface at the cell plasma membrane is an important first step. Probing the activity at the perimeter of a cell can improve understanding of the biocidal behavior of nanoparticles.

It is often difficult to probe changes to the cell plasma membrane in living organisms because of the complexity of the system and the difficulty controlling for variables. Thus, model membranes have been developed to analyze the changes induced by AgNPs on the cell plasma membrane, allowing for a more careful study of specific factors that control this interaction. AgNP-specific interactions with model membranes have been readily studied: nanoparticle binding at the membrane has been found to cause

restructuring through adhesion,^{61–63} pore formation and leakage,^{64–66} translocation of the particle beyond the membrane or penetration between the bilayer,^{67–70} and extraction of phospholipids.^{64,71} Previous literature has shown that observations from model membrane systems correlate well with *in vivo* effects on organisms.^{65,72}

1.2.1: *Caulobacter crescentus* Background and Relevance

A potentially useful model organism for understanding membrane-specific interactions of AgNPs is *Caulobacter crescentus*. *C. crescentus* is an oligotrophic alphaproteobacterium that can often be found in nutrient-poor environs such as wastewater treatment and sewage systems.^{73,74} These habitats coincide with the runoff sources where AgNPs are typically found as they are released into the environment after washing or improper disposal.⁷⁵ This coincidence suggests the potential applicability of *C. crescentus* as a model organism for understanding the interactions of AgNPs with bacteria. Furthermore, *C. crescentus* has a relatively simple membrane composition that can be easily mimicked in a laboratory setting. Its membrane primarily consists of two phospholipids, phosphatidylglycerol (PG) and cardiolipin (CL).⁷⁶

The unique characteristics of *C. crescentus* not only allow comparisons to other alpha-proteobacteria, but also make it an ideal organism to study membrane interactions of AgNPs due to the extension of its surface area through a dimorphic life cycle, shown in **Figure 1**. These bacteria alternate between a stalked cell form, characterized by the presence of a prostheca (stalk) and holdfast, and a swarmer cell form, characterized by a flagellum and pili at a single pole. The stalked cell is a base for the asymmetric division of the cell, producing a genetically identical daughter swarmer cell. The swarmer cell moves throughout the environment, mainly improving expansion and dispersion

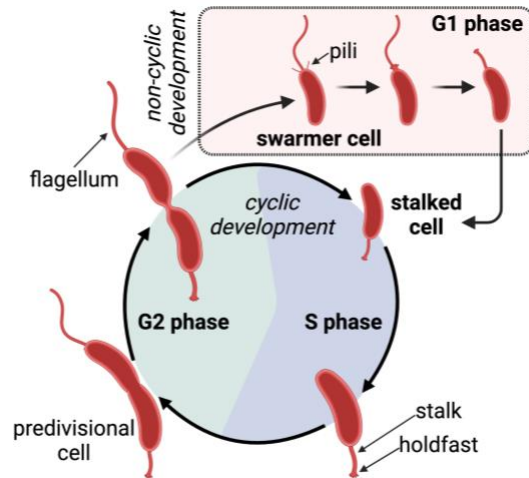


Figure 1. Schematic of the dimorphous life cycle of *C. crescentus* including stalked and swarmer cells. Created with Biorender.com

capabilities of the colony to sites with better nutrient availability.⁷⁷ After some time, the swarmer cell sheds the pili and flagellum, grows a prostheca, and attaches itself to a surface using the holdfast, where it can begin to once again produce daughter cells, marking the completion of this life cycle. The holdfast is an extremely powerful biological adhesive excreted by the bacteria allowing for biofilm creation and the establishment of a stable colony. Importantly, the prostheca mostly lacks any cytoplasmic material and is almost entirely composed of just the cell membrane and cell wall; this greatly extended membrane allows improved nutrient uptake through the added surface area.⁷⁸ The dimorphic life cycle described here has often been described as a bet-hedging strategy, relying on both the establishment of a secure colony that continues to produce daughter cells in the stalked form, as well as the ability to expand and disperse the colony through the swarmer form.^{77,79}

C. crescentus has been hailed as a “model system extraordinaire” in recent literature due to its unique and diverse characteristics, including its morphology and asymmetric process of cell division. As an alpha-proteobacteria, it has many similarities to other species within its class, allowing experimental findings to be generalized.⁷⁹ It is a good model for uncommon bacteria species with diverse characteristics.⁷⁷ For example, the family *Hyphomonadaceae* are also alpha-proteobacteria found in similar environments to *C. crescentus*, and one species in particular, the *Hirschia baltica*, has been found to have similar characteristics, including holdfasts and prosthecae as well as asymmetric cell division cycles.^{77,80} These findings suggest the applicability of these three cell features as useful in the survival of oligotrophic bacteria, and may allow trends found in *C. crescentus* to be generalized across other alpha-proteobacteria sharing its characteristics.

1.2.2: Modeling the Cell Plasma Membrane

The cell plasma membrane is a complex system that is commonly described as a “fluid mosaic” due to its behavior and composition. It is mainly composed of a phospholipid bilayer, comprising approximately 50% of the mass of the membrane in most eukaryotic cells,⁵⁷ as well as a wide variety of peripheral and integral proteins inserted into the membrane that support essential biological functions and allow for transport of molecules across the membrane.⁵⁸ The membrane structure of bacteria is yet more complicated, with many bacteria having both an inner cell plasma membrane as well as a cell wall, composed of the outer cell plasma membrane and a peptidoglycan protective layer. Outside of the cell wall, many bacteria have an S-layer, an adhered layer of proteins to protect the cell and help maintain its shape and rigidity.⁸¹ This system can

be extremely complex to model, further complicated by the shape and size of cells. Most bacterial cells are 0.4-3 μm^3 by volume and vary greatly in shape.⁸² However, from the perspective of a molecule approaching the cell plasma membrane they appear roughly planar due to their large size. Thus, it is difficult to create membranes that mimic complexity of the cell plasma membrane, both in the complex system of macromolecules observed *in vivo* as well as the rough planarity as seen by small molecules and the properties of a biological phospholipid bilayer, such as lipid lateral mobility and membrane permeability. Current research has suggested several potential model membrane systems that balance the factors of membrane complexity, planarity, and permeability with the ability to create replicable and analyzable structures in a laboratory setting.^{59,68,72}

Of the many available model systems, the most widely used are Langmuir-Blodgett lipid monolayers, supported lipid bilayers (SLBs), and liposomes.^{59,65} Langmuir-Blodgett monolayers are commonly used in microscopy studies to probe changes in phase and thickness. These monolayers are formed in a Langmuir trough at the air-water interface, preferentially making the hydrophobic lipid tails face into the air while the hydrophilic heads are submerged into the water. In interactions with nanoparticles, this model system can be readily used to understand both adhesion to and penetration of the monolayer. Current research has found cationic⁸³ and hydrophobic⁸⁴ particles to have more infiltratory interactions with the monolayer. Additionally, this model system can be used to probe pore formation of the membrane, where studies have similarly found the greater disrupting activity of cationic nanoparticles.⁸⁵ While the Langmuir-Blodgett monolayer makes it easy to study membrane properties using

microscopy, it is disadvantaged by inaccurately mimicking the bilayer interface as a monolayer and also by having partial contact with air, factors which may impact the behavior of the membrane surface and its interactions.⁵⁹

Supported lipid bilayers (SLBs) deposit a lipid bilayer onto a technique-sensitive surface and can be used in a variety of methods including quartz crystal microbalance with dissipation (QCM-D), atomic force microscopy, and several electrochemical techniques. These model membrane systems can be used to study pore formation and structural defect formation⁸⁶ as well as adhesion of particles to the membrane.^{62,63,87} Like for the Langmuir-Blodgett monolayer membrane system, studies using SLBs have confirmed the greater disrupting activity of cationic particles.^{87,88} Despite the wide array of techniques and measurements that can be performed using this system, the data collected using SLBs are greatly limited by the fact that these membranes are fixed to a solid support, which reduces mobility and lateral diffusion of phospholipids within the bilayer.^{59,65} Curvature and mobility of lipids greatly impact the behavior of a membrane, including their interactions with small molecules and particles.^{59,64,68} Thus, it is important to develop a model membrane system that better incorporates the curvature seen in cell plasma membranes.

The final model membrane system commonly used in research is the liposome. Liposomes, also called vesicles, are self-assembling spheres composed of a phospholipid bilayer. They can be generated through a variety of methods that control for size and lamellarity, or the number of bilayers in the membrane. Liposomes are classified according to these parameters: small unilamellar vesicles (SUVs) are up to 100 nm in diameter, large unilamellar vesicles (LUVs) have a diameter between 100 nm and 1 μm ,

giant unilamellar vesicles (GUVs) are over 1 μm in diameter, and multilamellar vesicles (MLVs) have two or more bilayers in their membranes.⁶⁸ In their interaction with AgNPs, liposomes can be used to probe a variety of behavior changes, including leakage of cellular contents due to nanoparticle adhesion or pore formation,⁶⁶ changes to membrane fluidity and melting temperature,^{69,70,89} changes to liposome size due to nanoparticle adhesion or encapsulation,⁷² and lipid extraction by the nanoparticles.⁷¹ Studies conducted using liposomes have also shown good correlation with *in vivo* studies.⁹⁰ In contrast to the planar model systems described earlier, liposomes of all sizes have laterally mobile lipids and some degree of membrane curvature. However, both SUVs and LUVs overcompensate for this curvature as compared to cells, which may impact their behavior and interactions due to their relative size as compared to small molecules and particles. Additionally, liposomes with proteins embedded within the membrane have been synthesized,⁶⁵ demonstrating an initial effort to replicate the degree of complexity in the cell plasma membrane.

1.3: The Eco-Corona

AgNPs undergo a wide variety of environmental transformations (see Section 1.1), but their ability to form eco-coronas is unique and requires special consideration. Eco-coronas can include a variety of biomolecules, including proteins, lipids, and metabolites, as well as environmental molecules like NOM. Eco-coronas have been extensively studied and characterized in the nanoparticle field. The importance of the changes they impart on nanoparticle properties and interactions are rapidly becoming more apparent in current research. First, through physical adsorption to the nanoparticle surface, eco-corona constituents may increase the surface area and diameter of AgNPs.

Additionally, through charge screening, adsorbates typically minimize repulsive surface potentials between particles, leading to aggregation. These changes are likely to have many downhill effects on the electrostatic and physical behavior of nanoparticles in complex systems. Eco-coronas are known to modulate AgNP behavior in a size- and concentration-dependent manner, affecting their dissolution, agglomeration, and stability.¹⁴ Eco-coronas can enhance oxidative dissolution of AgNPs^{40,44} as well as increase their aggregation behavior.⁹¹ These transformations can both increase⁹² and decrease⁴¹ colloidal stability of AgNPs, dependent on the concentrations and compositions of the systems.⁴⁴

Eco-corona formation is non-specific, with AgNPs picking up adsorbates as they travel through complex systems that then reflect the previous fate and transport of an AgNP.¹⁴ The path-dependent nature of complex corona formation has led to the idea of “stealth coronas,”⁹³ which have been exploited in medicine. If an eco-corona is composed of familiar biomolecules, such as signaling proteins native to a given cell, it has been suggested that the nanoparticle is more likely to be recognized as non-harmful by any defense mechanisms. In medicine, this discovery has been used for advancements in drug delivery, using stealth coronas to allow direct-to-cell introduction of therapeutic nanoparticles.⁹⁴ However, in an environmental context, this has raised concerns about the enhanced toxicity generated by an appropriate stealth eco-corona, which could increase nanoparticle recognition by living organisms and lead to augmented cell damage.

The presence of an eco-corona on AgNPs has been seen to greatly impact their interaction with cells, however contradictory results between studies have been obtained. Gunsolus et. al found that the toxicity of AgNPs pre-coated with an eco-corona composed

of NOM enhanced the colloidal stability of their nanoparticles and reduced their toxicity on a simple bacterial model organism.⁹⁵ In contrast, Shannahan et. al reported that coronated AgNPs had reduced cytotoxicity together with increased cellular uptake, potentially leading to a more toxic downhill effect on bacteria.⁹⁶ To further complicate the matter, Wang et. al reported that AgNPs with a protein corona promoted toxicity to *E. coli* but upon addition of NOM, their toxicity decreased.⁹⁷ It is clear from previous work that the effect of an eco-corona on the toxicity of nanoparticles is complicated and multifaceted, and needs to be better understood. More careful analytical work must be performed in order to fully elucidate the interactions of coronated AgNPs with the cell plasma membrane.

1.4: Proposed Work

This study endeavors to begin to address the lack of relevant environmental model systems for prediction of the real-world behavior of AgNPs and their specific interactions with lipid membranes. The model organism *C. crescentus* was chosen to simulate the environmental reactivity of AgNPs, including *in vivo* studies to explore the toxic effects of AgNPs on *C. crescentus* and *in vitro* studies using model liposomes to begin investigating possible mechanisms of toxicity. *C. crescentus* is a representative organism that effectively models a potential path taken by AgNPs after release into the environment, due to the overlap of their habitat with waste streams containing AgNPs.

The current study has three aims: (1) to understand the antibacterial activity of AgNPs on *C. crescentus*, (2) to understand the effect of an appropriate eco-corona on the interactions of AgNPs with a model cell plasma membrane, and (3) to correlate the *in vivo* toxicity of both AgNPs and coronated AgNPs with model membrane results. AgNPs

with a diameter of 10 nm were chosen for all studies to better simulate the relative sizes between a cell and a nanoparticle in the environment. For the first part of this study, the impact of AgNPs on the total growth and growth rate of *C. crescentus* was quantified. Then, AgNP eco-coronas were formed using spent medium derived from *C. crescentus* to best imitate relevant environmental molecules that AgNPs would encounter. Finally, the impact of coronated AgNPs on the total growth and growth rate of *C. crescentus* was quantified.

For the second and final part of this study, the inhibition of total *C. crescentus* growth and decreases in growth rate seen in earlier phases of the work were correlated with direct mechanistic impacts observed using model membrane systems. Liposomes mimicking the *C. crescentus* membrane composition were synthesized, incubated with bare and coronated AgNPs, and analyzed using dynamic light scattering (DLS) and fluorescence anisotropy. Together, this project aspires to contribute to environmental relevance in AgNP and membrane studies, providing a comprehensive understanding of the toxicity of AgNPs on biological membranes and the effects of an eco-corona on this interaction.

Chapter 2: Materials and Methods

2.1: Chemicals

Calcium chloride dihydrate (99%+), 1,6-diphenyl-1,3,5-hexatriene (DPH, 98%), Sodium 2-(4-(2-hydroxyethyl)piperazin-1-yl)ethanesulfonate (HEPES, 99%), Bacto™ Peptone, magnesium sulfate heptahydrate (99+%), and yeast extract were purchased from Thermo Fisher Scientific (Heysham, England). Bacto™ Agar was purchased from Becton, Dickinson and Company (Sparks, MA). Ethylenediaminetetraacetic acid (EDTA, 99+%), potassium chloride (99+%), and Trizma® base (Tris, 99.9+%) were obtained from Sigma-Aldrich (St. Louis, MO). BioPure citrate-stabilized AgNPs with a nominal diameter of 10 nm were purchased from NanoComposix and were provided at a concentration of 1 mg mL⁻¹ suspended in a 2 mM sodium citrate solution (La Jolla, CA). Particles from lot number JRS0017 were used for all *in vivo* and time-resolved studies, but some optimization work was done with particles from lot number MPP0024. All AgNPs were handled in a dark room to prevent UV-induced transformations (e.g., dissolution and aggregation).

Liposomes were prepared in a buffer solution containing 50 mM Tris, 100 mM KCl, and 1 mM EDTA (pH = 7.8; herein, “extruder buffer”) in Millipore water (18.2 MΩ.cm at 25 °C). All other experiments, with the exception of the bacterial growth study, were carried out in a buffer solution composed of 20 mM HEPES and 1 mM EDTA (pH = 7.4; herein, “HEPES/EDTA buffer”) prepared in Millipore water. The pH of each buffer solution was adjusted through dropwise addition of 0.1 or 1.0 M hydrochloric acid or sodium hydroxide.

A working stock solution of AgNPs was prepared to a final concentration of 10 mg L⁻¹ in HEPES/EDTA buffer. To prevent aggregation, the as-received stock solution of AgNPs was sonicated for five minutes and vortexed for one minute before preparing the working stock. The working stock was prepared fresh each week and was stored at 4 °C and handled in the dark.

Phosphatidylglycerol (PG, 18:1) and cardiolipin (CL, 18:1) were obtained from Avanti Polar Lipids (Alabaster, AL). The phospholipids were in chloroform at concentrations of 0.5 and 2 mg mL⁻¹ respectively. Once the ampule was opened, phospholipids were immediately dried down into a lipid film for later re-hydration. Lipid films were made by drying down and lyophilizing the appropriate ratios of phospholipids in order to obtain a final liposome composition of 9:1 PG to CL, with a final total lipid concentration of 10 mM once the films were re-hydrated to 500 µL. For the lipid films to be used in the anisotropy experiment, a working stock of 100 µM of the fluorescent probe DPH was prepared in acetone. The DPH stock solution was handled in a dark room to prevent UV-induced decomposition. To prepare lipid films for anisotropy, DPH was added and dried down on top of the film so that the final concentration would be 200 nM with a probe:lipid ratio of 1:50,000 once the films were re-hydrated to 500 µL. All lipid films were stored in glass vials wrapped with Parafilm at -20 °C until re-hydration.

2.2: Culturing *Caulobacter crescentus*

C. crescentus were grown with peptone yeast-extract (PYE) growth medium, composed of 0.2% w/v Bacto Peptone®, 0.1% w/v yeast extract, 0.5 mM CaCl₂, and 1 mM MgSO₄ in Millipore water. Additionally, PYE prepared with 1.5% BactoAgar was

used to pour agar plates. The agar-containing medium was first autoclaved at 240 °C for 30 minutes and after two hours of cooling was poured into petri dishes using the sterile method to a solution height of approximately 1 cm. The agar plates were covered and allowed to cool overnight before they were stored at 4 °C. Fresh agar plates were prepared every two months.

C. crescentus strain NA1000 was graciously provided by the laboratory of Dr. Michael Laub at the Massachusetts Institute of Technology. Glycerol stocks stored at -80 °C were used to streak starter cultures. Then, the starter cultures were allowed to grow at room temperature overnight before incubation at 30 °C for two days. The plate stocks were then stored at 4 °C covered in Parafilm and were re-plated every week.

2.3: *In Vivo* Toxicity Studies

Starter broth cultures were inoculated from plate stocks by scooping two lines of bacteria from the plate with an autoclaved wooden pick and dipping the pick into 500 mL of PYE broth in an autoclaved 500 mL baffled flask. The baffled flask was then covered with aluminum foil and incubated at 30 °C with continuous shaking at 210 rpm overnight. The optical density at 600 nm (OD₆₀₀) was taken to measure the growth of the culture. OD₆₀₀ measurements were recorded using an Ultraspec 10 spectrophotometer from Amersham Biosciences (Amersham, UK). For all OD₆₀₀ measurements, 500 µL of the culture were withdrawn and analyzed in disposable polystyrene cuvettes. A cuvette containing 1 mL of PYE broth was used as the blank. To ensure full growth of the starter culture, its OD₆₀₀ was checked and confirmed to be over 1.2 before proceeding with the toxicity study.

Cultures for the growth curve experiment were grown in 125 mL autoclaved baffled flasks. Using autoclaved graduated cylinders, 25 mL of PYE broth and 4 mL of starter culture were added to the baffled flasks using the sterile method. Then, either AgNPs or coronated “spent medium-AgNPs” (SM-AgNPs, see section 2.4) were added so the final concentration was 2 mg L⁻¹. The control cultures (with no AgNPs) received an equivalent volume of PYE broth so that the total volume was the same in all experiments. All cultures were grown in triplicate. The OD₆₀₀ values at the start of the experiment were taken, then the cultures were incubated at 30 °C with continuous shaking at 210 rpm. Approximately every thirty minutes the OD₆₀₀ values of the cultures were measured. Measurements continued until culture growth plateaued, usually around OD₆₀₀ = 1.3. For all cultures grown with the presence of AgNPs, the OD₆₀₀ of a control cuvette containing PYE and 2 mg L⁻¹ AgNPs or SM-AgNPs was also measured, and the cuvette was also incubated in the same conditions as the cultures.

Data from the toxicity study were analyzed using the Boltzmann sigmoid distribution, according to:

$$y = \frac{A_1 - A_2}{1 + e^{-\frac{x - x_0}{dx}}} + A_2 \quad (2)$$

where x is the time since inoculation of the culture, y is the OD₆₀₀ of the culture, A_1 is the initial absorbance value, A_2 is the final absorbance value, x_0 is the center of the sigmoidal curve (i.e. the time of 50% growth), and dx is the time constant which is inversely related to the rate of maximum growth. The Boltzmann sigmoid distribution, also called the logistic model, is a frequently used model function to parameterize dose-response curves due to the simplicity of its fit. This model, in comparison to other similar model

functions, can be used to fit data with minimal computational expense, however, it can often parameterize unrealistic A_1 and A_2 values with limited data input, and this in turn can lead to a biased estimate of the x_0 parameter.⁹⁸

2.4: Eco-Corona Formation

Spent PYE medium was isolated from *C. crescentus* by growing the culture at 30 °C with continuous shaking at 210 rpm, as previously described. The OD₆₀₀ of the culture was continuously monitored, and after reaching the desired culture density of 1.0, a 30 mL aliquot was taken. This aliquot was spun down for 24 minutes at 3500×g, and then the supernatant was removed and filtered using vacuum filtration with a 0.2 µm filter. A 0.5 mL aliquot of the filtrate was re-plated to ensure all bacterial growth had been removed from the medium. The spent PYE medium was then stored in aliquoted sterile containers at -20 °C until needed.

To form an eco-corona around AgNPs, an aliquot of spent medium was thawed at room temperature, then vortexed for 10 seconds. The spent medium was then diluted 1:1000 in HEPES/EDTA buffer to match environmentally relevant concentrations. Then, AgNPs were added to a final concentration of 10 mg L⁻¹ for UV-Vis, DLS, and fluorescence anisotropy studies or to a concentration of 58 mg L⁻¹ for bacterial growth studies. Note that a concentration of 58 mg L⁻¹ was needed for the growth studies such that when diluted in the final volume of PYE, the AgNPs had a concentration of 2 mg L⁻¹. SM-AgNPs were incubated at room temperature overnight in a dark room to ensure full corona formation before analysis. After incubating overnight, the SM-AgNPs were either used immediately in an experiment at their prepared concentration or diluted to the appropriate final concentration for the experiment. SM-AgNPs that were not used

immediately following overnight incubation were stored at 4 °C in the dark and used for no more than one week.

2.5: Liposome Preparation

Liposomes were synthesized using the extrusion method. The liposome extruder is shown in **Figure 2**. The extruder apparatus sandwiches a polycarbonate filter with a 200 nm pore size between filter supports and allows two lipid air-tight syringes to be inserted on either side to pass a solution through multiple times and ensure uniform size distribution. The extruder was primed with 30 μL of extrusion buffer. The apparatus was checked for leaks by passage of HEPES/EDTA buffer, and this process also allowed the void space of the extruder to be calculated. If the void space was found to be under 100 μL , the extrusion could be performed; if the void space was over 100 μL , the extruder was disassembled, washed, and reassembled.

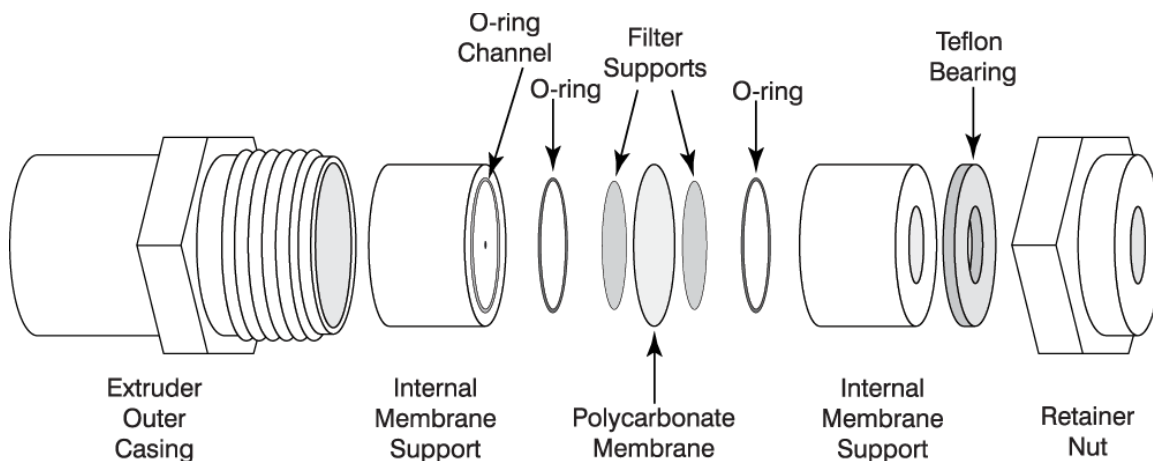


Figure 2. Schematic of the extruder apparatus used in liposome preparation. Two glass syringes were inserted in either side of the apparatus and used to push the lipid solution through a 200 nm polycarbonate filter to extrude liposomes of a defined size.

Lipid films were re-hydrated by incubating them for 30 minutes in 500 μ L of HEPES/EDTA buffer. Then, the resuspended lipids were vortexed, and bath sonicated for five minutes. The films were fully re-hydrated through three freeze-thaw cycles, which included ten seconds of vortexing followed by ten seconds submerged in a dry ice-acetone bath and finally fifteen seconds in a hot water bath. The resuspended lipids were then transferred from a glass vial to a 1.5 mL Eppendorf tube.

The lipid suspension was transferred to an air-tight extruder syringe and passed fifteen times through the extruder apparatus. The apparatus was fully cleaned with Millipore water and dried between extrusions. Final liposome solutions were stored at 4 $^{\circ}$ C and used for no more than one week. To ensure homogeneity and prevent aggregation, all liposome stocks were vortexed for ten seconds prior to sample preparation.

2.6: Size and Surface Potential Characterization by DLS

DLS measurements were collected using a Zetasizer Nano ZS from Malvern Panalytical (Worcestershire, UK). The instrument was allowed to warm up for at least twenty minutes before data collection. For all DLS size measurements, disposable polystyrene cuvettes were rinsed twice with HEPES/EDTA buffer, which had been filtered twice using 0.2 μ m nylon syringe filters. Semi-micro cuvettes (1 cm pathlength) were used for hydrodynamic diameter measurements and macro cuvettes (1 cm pathlength) were used for zeta potential measurements. All samples were prepared in triplicate directly in disposable cuvettes. For the zeta potential measurements, a Pd dip cell was inserted. The dip cell was washed thoroughly with Millipore water between measurements.

2.6.1: Liposome Characterization

Liposomes were diluted in HEPES/EDTA buffer to a final total lipid concentration of 100 μM . The cuvettes were vortexed for ten seconds before insertion into the DLS cuvette holder. Liposomes were analyzed at 30 °C with an equilibration time of 120 seconds. The refractive index was set to 1.369 and the absorption at 633 nm was set to 0. Normal resolution processing mode was used to process all data.

2.6.2: AgNP Characterization

AgNPs and SM-AgNPs were diluted in HEPES/EDTA buffer to a final concentration of 500 $\mu\text{g L}^{-1}$. The cuvettes were vortexed for ten seconds before insertion into the DLS cuvette holder. AgNPs were analyzed at 30 °C with an equilibration time of 120 seconds and a refractive index set to 1.330 and an absorption at 633 nm of 0.010. Normal resolution processing mode was used to process all data.

2.7: UV-Vis Characterization of AgNPs

AgNPs and SM-AgNPs were diluted in HEPES/EDTA buffer to a final concentration of 3.33 mg L^{-1} in order to have a high enough absorbance to be detected but not to overwhelm the detector. Samples were thoroughly vortexed before the measurement. Spectra were recorded from 350 to 800 nm, with the scan rate set to 0.1 nm/second. HEPES/EDTA buffer was used to zero the instrument and for baseline subtraction. Samples were prepared in triplicate and the λ_{max} values were obtained.

2.8: Probing Time-dependent Liposome Size Changes with DLS

Similar to the sample preparation for DLS characterization, three disposable semi-micro polystyrene cuvettes were rinsed twice with double-filtered HEPES/EDTA buffer.

At time 0, liposome stocks were vortexed and diluted to 100 μM total lipid concentration in HEPES/EDTA and AgNPs and SM-AgNPs were added from their respective working stock solutions (10 mg L^{-1}) to a final concentration of 2 mg L^{-1} . The three cuvettes were then submerged in a 30 $^{\circ}\text{C}$ water bath in a dark room and allowed to incubate through the duration of the study. At two-hour increments for ten hours, the three cuvettes were withdrawn one at a time from the water bath and analyzed using DLS. An additional measurement was made at 24 hours. As before, the cuvette was vortexed before being placed into the cuvette holder. All DLS parameters are the same as listed above.

2.9: Probing Time-dependent Membrane Fluidity Changes with Fluorescence

Anisotropy

At time 0, liposomes embedded with the fluorescent probe DPH were diluted to 100 μM total lipid concentration and 2 nM DPH concentration in HEPES/EDTA and AgNPs and SM-AgNPs were added in from the working stock solutions (10 mg L^{-1}) to a final concentration of 2 mg L^{-1} in Eppendorf tubes. At each concentration tested, samples were prepared in triplicate. The three tubes were then submerged in a 30 $^{\circ}\text{C}$ water bath in a dark room and allowed to incubate through the duration of the study. At two-hour increments for ten hours, the samples were withdrawn one at a time to be analyzed using fluorescence anisotropy. An additional measurement was made at 24 hours. The samples were pipetted into a macro fluorescence cuvette (1 cm pathlength), analyzed, pipetted back into the Eppendorf tubes, and then the cuvette was rinsed twice with HEPES/EDTA buffer before the next sample was analyzed. Fluorescence anisotropy measurements were recorded using a QuantaMaster Steady-state Fluorometer with polarizer accessories from Photon Technology International, Inc. (Birmingham, NJ). The excitation wavelength was

set to 350 nm and the emission wavelength was set to 452 nm. The lamp was allowed to warm up for at least 15 minutes before any measurements were recorded. All slit widths were set to 1.25 mm. All fluorescence anisotropy measurements were recorded at 30 °C.

Chapter 3: AgNP Toxicity to *C. crescentus* is Modulated by the Presence of an Eco-Corona

3.1: Characterization of AgNPs and SM-AgNPs with DLS and UV-Vis

DLS is used to measure the hydrodynamic diameter (d_H) and zeta potential of large particles suspended in solution through their Brownian motion. DLS is a common technique used for characterization of liposomes⁹⁹ and AgNPs¹⁰⁰ alike. Brownian, or random, motion describes the path taken by particles in solution as influenced by their collisions with other particles and solvent molecules. The extent of this motion over time correlates strongly with particle size, with smaller particles having a higher degree of Brownian motion than larger particles. In this technique, a laser is directed through a solution containing suspended particles, and the time-dependent intensity of scattering, indicative of the Brownian motion of the particles, is then correlated with their size to produce a size histogram.^{100,101} Since the nanoparticles have a nominal diameter of 10 nm, which is at the limit of detection of the DLS, the average size data (Z-ave) which is typically used to describe the hydrodynamic diameter of the particles was not an indicative metric of the monodisperse particle size in this case.¹⁰² Instead, only the larger aggregates were observed by DLS. It is important to note that the core diameter provided by the manufacturer obtained through transmission electron microscopy of 9.1 ± 1.3 nm does not align well with the results obtained through DLS, suggesting the formation of AgNP aggregates in these conditions and emphasizing the limit of detection of this technique.

The size of the bare freshly prepared AgNPs was 280 ± 40 nm, with a very large polydispersity index (PdI) of 0.29 ± 0.04 , indicating a largely heterogeneous population

of AgNPs. After 24 hours of incubation in spent medium, the initial size of the SM-AgNPs was 120 ± 60 nm with a PDI of 0.20 ± 0.01 . Note that the DLS results of 10 nm AgNPs must be carefully analyzed, as the DLS is unable to detect a monodisperse particle peak. However, these data suggest the stabilizing role of the eco-corona in preventing AgNP aggregation, both through the lower average size of the particles and the more homogeneous sample size. Next, to simulate conditions used in the DLS and fluorescence anisotropy time-resolved studies, the AgNPs and SM-AgNPs were incubated at 30 °C for an additional 24 hours, after which their sizes were re-examined. The bare AgNPs after 24 hours had a diameter of 290 ± 60 nm with a PDI of 0.42 ± 0.09 , showing further aggregation and heterogeneity of the particle sizes. After 24 hours, the SM-AgNPs had a diameter of 220 ± 50 nm and a PDI of 0.3 ± 0.1 , also showing further aggregation, though not to the extent of the bare AgNPs (**Table 1**). Together, these results support the formation of the eco-corona and demonstrate its stabilizing effect against temperature induced AgNP aggregation.

Table 1. Experimental AgNP hydrodynamic diameters and zeta potentials, obtained through DLS.^a

	AgNPs		SM-AgNPs	
	0 hrs	24 hrs	0 hrs	24 hrs
d_{AgNP} (nm)	280 ± 40	290 ± 60	120 ± 60	220 ± 50
PDI	0.29 ± 0.04	0.42 ± 0.09	0.20 ± 0.01	0.3 ± 0.1
ζ (mV)	-37 ± 3		-32 ± 3	

^aAgNPs were analyzed following initial sample preparation (0 hrs) or after 24 hrs incubation at 30 °C

Zeta potential (ζ) measurements of the particles were also obtained to confirm formation of an eco-corona. For zeta potential measurements, the time-dependent intensity of scattering by the particles is measured while they move in response to a generated electric field.^{103,104} The zeta potential of the AgNPs increased by 5 mV upon incubation in the spent medium (**Table 1**), indicating the formation of an eco-corona. This change in zeta potential was slightly statistically significant (p-value < 0.1). As a control experiment, the zeta potential of the undiluted spent medium was obtained, and a value of -10.3 mV was recorded. Since the spent medium is less negatively charged than AgNPs alone, the adsorption of spent medium components to the nanoparticle surface can effectively screen the charge.

Eco-corona formation was further probed using UV-Vis spectroscopy. It is well known that AgNPs experience a phenomenon known as localized surface plasmon resonance (LSPR), an optical property due to their small size that leads to their ability to be measured using optical spectroscopy. LSPR bands occur when the oscillation of the electron cloud of the nanoparticle is in resonance with the frequency of the incident light, with larger particles having longer wavelength LSPR bands.^{105,106} After incubation at room temperature for 24 hours, the λ_{\max} value of the SM-AgNPs was compared to a freshly made stock of AgNPs. The λ_{\max} of the bare AgNPs was 396.0 ± 0.4 nm and shifted to 397.9 ± 0.1 nm for the SM-AgNPs (**Figure 3**). The λ_{\max} of 396.0 ± 0.4 nm is typical of AgNPs of a nominal diameter of 10 nm, with the manufacturer reporting a slightly lower value of 390 nm. This clear red-shift in the LSPR band of the AgNPs upon incubation in spent medium further shows the formation of the eco-corona. However, while large aggregates were seen in the DLS size distributions, the presence of these

aggregates is not observed in the UV-Vis spectrum (**Figure 3A**), where aggregated nanoparticles would have an LSPR band around 600-800 nm, depending on the size of the aggregate. These conflicting data highlight the limitations of DLS at small particle diameters; from these data alone it is difficult to conclusively determine effects of the eco-corona on AgNP size.

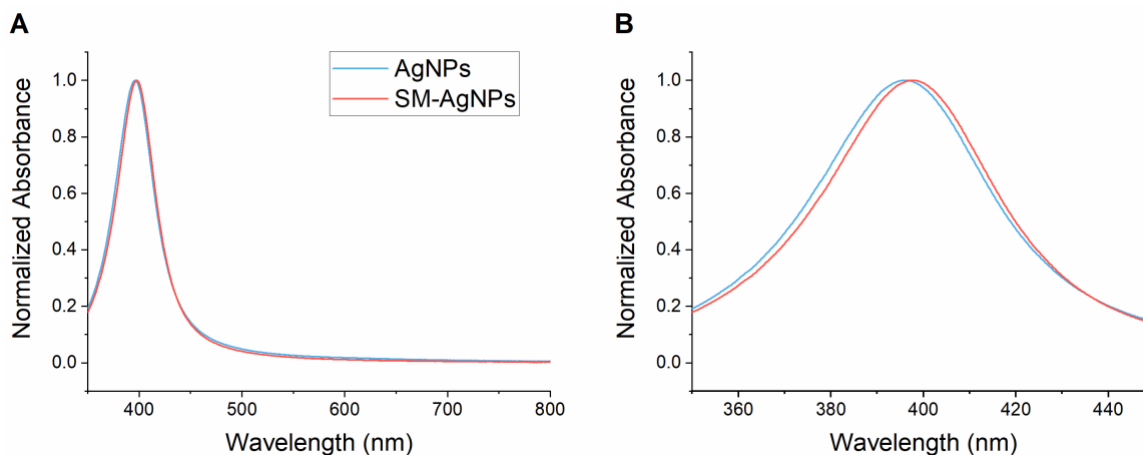


Figure 3. Representative UV-Vis spectra of AgNPs and SM-AgNPs prior to incubation at 30 °C. All samples were prepared to 3.33 mg L⁻¹. AgNPs were prepared in HEPES/EDTA buffer at pH 7.4, and SM-AgNPs were added to 1:1000 dilute spent medium in HEPES/EDTA buffer and incubated for 24 hours at room temperature. **(A)** Full UV-Vis spectra. **(B)** Section of the UV-Vis spectra showing the shift in λ_{\max} upon eco-corona formation.

Then, to simulate conditions of the time-resolved DLS and fluorescence anisotropy studies, both the bare AgNPs and SM-AgNPs were incubated at 30 °C for 24 hours. The λ_{\max} of the bare AgNPs after 24 hours was 395.5 ± 0.3 whereas the λ_{\max} of the SM-AgNPs after 24 hours was 396.3 ± 0.1 nm. After these additional 24 hours, the redshift in the AgNPs LSPR band is still apparent, although less dramatic. The slight decrease in the λ_{\max} in both cases after 24 hours at 30 °C may be due to dissolution,

although it is difficult to be certain. Overall, the AgNPs and SM-AgNPs maintain the same optical properties over 24 hours at 30 °C.

3.2: AgNPs and SM-AgNPs Induce Distinct Effects on *C. crescentus* Growth

To evaluate the toxicity of AgNPs on living organisms, it is important not only to fully evaluate the mechanism of interaction using model membrane systems, but also to directly measure effects on cells *in vivo*. Sondi et. al used a comparison of the growth curves of two *E. coli* cultures, one grown under standard conditions, and one grown in the presence of AgNPs. This study allowed both the rate of growth of the cells and their maximum OD₆₀₀ to be compared as valuable indicators of cell viability and the effects of toxicity.³⁶ In comparing the results obtained through model membrane systems and *in vivo* toxicity studies, both the mechanism and the impact of toxicity on cells can be thoroughly understood. In this study, *C. crescentus* were grown in triplicate alone, in the presence of 2 mg L⁻¹ AgNPs, and in the presence of 2 mg L⁻¹ SM-AgNPs to determine the *in vivo* effects of AgNPs and SM-AgNPs on *C. crescentus*. The OD₆₀₀ of the culture is indicative of the cell density.

Qualitatively, the bacteria grown in the presence of both types of AgNPs showed a delay in their growth, as seen by a horizontal shift in the curve along the time axis (**Figure 4**). To quantitatively understand the growth data, they were fit to the Boltzmann distribution to which they showed good agreement ($R^2 > 0.999$ in all cases). The mid-point of bacterial growth (x_0) was seen at 3.12 ± 0.05 hours for the control culture, 3.38 ± 0.06 hours for the culture grown with 2 mg L⁻¹ AgNPs, and 3.26 ± 0.06 hours for the culture grown with 2 mg L⁻¹ SM-AgNPs (**Table 2**). With the addition of nanoparticles, the time it takes for the culture to reach 50% growth is significantly delayed. In **Figure 4**,

the SM-AgNPs curve seems to be the furthest delayed, but this does not match with the quantitative x_0 values where SM-AgNP culture reached half growth between the control culture and the AgNP culture. This disagreement is an artifact of the Boltzmann distribution: because the SM-AgNP culture reaches a lower maximum optical density, the optical density where it reaches half growth is then shifted to a shorter time. While both the control and AgNPs cultures grew to a similar maximum optical density (A_2) of 1.19 ± 0.03 for the control and 1.18 ± 0.01 for the culture with AgNPs, the culture grown with SM-AgNPs only reached a maximum optical density of 1.08 ± 0.02 . This shows a significant reduction in the cell density, indicating that SM-AgNPs prevent the culture from reaching its optimal growth. The different initial optical densities (A_1) of the growth cultures can be attributed to fit errors, with the control culture starting at 0.01 ± 0.02 and the AgNP and SM-AgNP cultures starting at 0.12 ± 0.02 and 0.08 ± 0.01 , respectively. The observed initial optical densities are within statistical significance of each other, with the exception of the SM-AgNP culture and the control culture (**Table A1**). This difference in the starting values is likely due to the heterogeneity of the cultures with AgNPs prior to incubation and did not contribute to the overall trends described here. Additionally, the dx parameter of the Boltzmann sigmoidal distribution is inversely proportional to the slope at the maximum growth rate, with larger values corresponding to a shallower slope. The AgNPs culture grew at a significantly slower rate (1.16 ± 0.04) at its maximum growth rate compared to both the control culture (1.07 ± 0.08) and SM-AgNP cultures (1.04 ± 0.05) (**Table 2**).

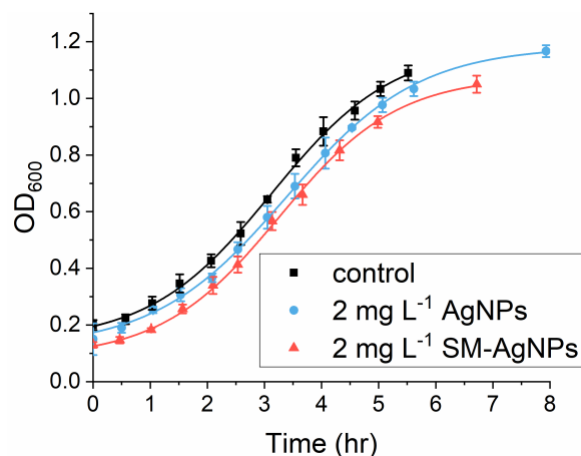


Figure 4. OD₆₀₀ growth curves of *C. crescentus* (control), in the presence of 2 mg L⁻¹ AgNPs, and in the presence of 2 mg L⁻¹ SM-AgNPs. All data points represent the average and standard deviation for three independent cultures. The absorbance signal of AgNPs alone in the cell medium was subtracted from each data point to account for any contribution of the AgNPs to the OD₆₀₀ signal. All data were fit to the Boltzmann distribution.

Table 2. Fit Parameters of Boltzmann sigmoidal distributions for the growth of *Caulobacter crescentus* in the presence of (SM-) AgNPs

Fit Parameter	Growth Condition		
	Control	2 mg L ⁻¹ AgNPs	2 mg L ⁻¹ SM-AgNPs
A_1	0.01 ± 0.02	0.12 ± 0.02	0.08 ± 0.01
A_2	1.19 ± 0.03	1.18 ± 0.01	1.08 ± 0.02
x_0 (hr)	3.12 ± 0.05	3.38 ± 0.06	3.26 ± 0.06
dx (hr ⁻¹)	1.07 ± 0.08	1.16 ± 0.04	1.04 ± 0.05
R^2	0.999	0.999	0.999

The growth of *C. crescentus* is significantly affected by the presence of AgNPs. Bare AgNPs delay the growth and slow the maximum growth rate, whereas SM-AgNPs delay the growth (although less so than AgNPs alone) and decrease the maximum optical density reached by the culture. Both types of NPs have detrimental effects on bacterial growth, but the manner of toxicity is modulated by the presence of an eco-corona.

Chapter 4: Development of a Model Membrane System Based on *C. crescentus* to Evaluate AgNP Reactivity

4.1: Modeling the *C. crescentus* Membrane with Large Unilamellar Vesicles

In order to mimic the membrane of *C. crescentus*, liposomes composed of 9:1 PG to CL were synthesized using the extrusion method (**Figure 5**), herein referred to as “PGCL liposomes”. To confirm that the liposomes created were of a uniform and replicable size and charge, DLS and zeta potential measurements were used to routinely characterize the liposomes. Three preparative replicates of liposomes were extruded, and these three sets were analyzed using DLS. The average size of the liposomes was 139 ± 1 nm, with a PDI of 0.17 ± 0.04 indicating that the extrusion process yields a relatively homogeneous sample with a small size distribution. To accurately measure the size of liposomes, vortexing for 10 seconds prior to analysis was a crucial step: the average size of the same liposomes without vortexing was 206 nm and showed a bimodal size

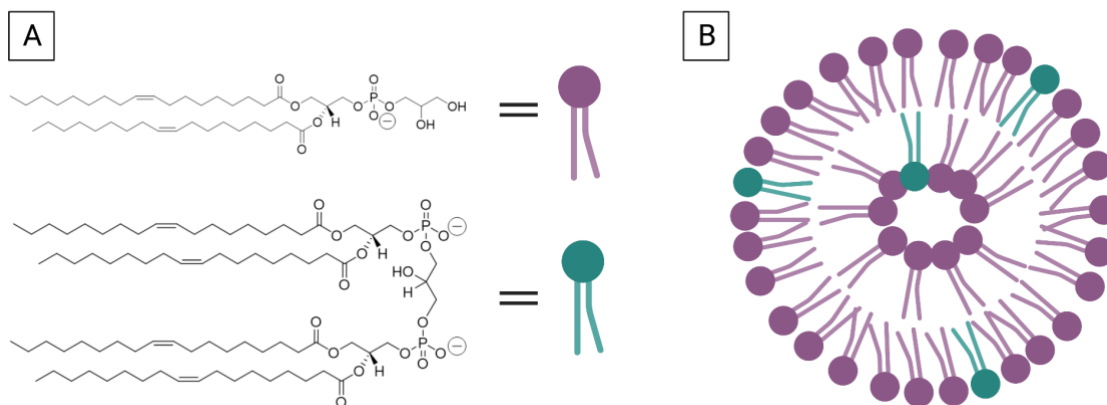


Figure 5. Schematic of the 9:1 PGCL large unilamellar vesicle. **(A)** Chemical structures of phospholipids phosphatidylglycerol (top, purple), and cardiolipin (bottom, teal). **(B)** Schematic of a formed 200 nm diameter liposome consisting of 9:1 PG to CL phospholipids. Created with Biorender.com

distribution with a large PDI of 0.28. The average zeta potential of the liposomes was -82 ± 3 mV. This highly negative zeta potential originates in the anionic head groups of the phospholipids, with the charged headgroups of PG contributing more to the net charge than the more highly anionic charged headgroups of CL due to their relative proportions (**Figure 5**). After showing the replicability of the extrusion method, it was then possible to measure changes in the liposome diameter upon addition of AgNPs. In understanding the interactions of nanoparticles with liposomes, DLS is a powerful technique to understand changes in size undergone by the liposome, indicative of AgNP adhesion to the surface or encapsulation.

4.2: Optimization of Fluorescence Anisotropy to Measure Changes in Membrane Fluidity

The cell plasma membrane can occupy two distinct phases: the gel phase, seen at lower temperatures with more compact phospholipid packing and a higher degree of rigidity; and the fluid phase, seen at higher temperatures with a looser packing and less rigidity.⁵⁸ The phase transition has been observed to be heavily impacted by the presence of AgNPs,^{70,107} which could explain some aspect of their toxicity through increasing the fluidity and permeability of the membrane. In the fluorescence anisotropy technique, the hydrophobic probe DPH was added to the membrane. This probe specifically segregates within the hydrophobic region of the phospholipid bilayer. DPH is soluble in acetone but not the aqueous buffer used in other parts of this study, so acetone was used to measure its fluorescence signal. DPH had a λ_{ex} of 347 nm and a λ_{em} of 440 nm in acetone (**Figure 6**). These values are similar to those reported by Sigma-Aldrich of a λ_{ex} of 350 nm and λ_{em} of 452 nm in methanol, and because of the good agreement of the values, 350/452

were chosen as the excitation and emission parameters for all future fluorescence anisotropy experiments.

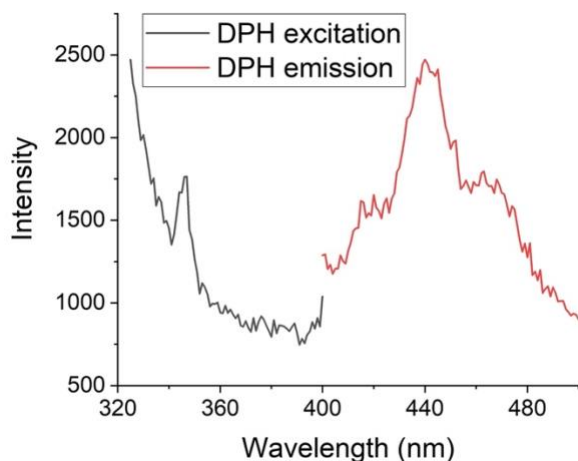


Figure 6. Excitation and emission spectra of 10 μM DPH in acetone.

DPH rotates polarized fluorescence light as a function of the rigidity of its environment, and the difference in vertically and horizontally polarized light can be characterized as anisotropy, $\langle r \rangle$.⁷⁰ Anisotropy is defined according to:

$$\langle r \rangle = \frac{I_{VV} - I_{VH}}{I_{VV} + G \cdot I_{VH}} \quad (3)$$

where I_{xy} is the intensity of the fluorescence signal, x is the polarization of the excitation wavelength along the vertical (V) or horizontal (H) axis, and y is the polarization of the emission wavelength. G is the correction factor, defined according to:

$$G = \frac{I_{HV}}{I_{HH}} \quad (4)$$

Fluorescence anisotropy is a very useful method to characterize the fluidity of the bilayer, and in terms of AgNP-bilayer interactions could readily be used to understand particle adhesion and permeability changes induced by interactions. In the current literature, fluorescence anisotropy has been used for determination of changes to the phase

transition temperature⁷⁰ and the degree of fluidity of the bilayer^{89,107} as a function of particle concentration. The goal of this study was to measure the change in fluorescence anisotropy over time, by incubating a liposome with DPH embedded within the membrane with AgNPs or SM-AgNPs in a hot water bath over a period of 24 hours and periodically measuring the anisotropy.

To optimize the conditions of fluorescence anisotropy, the anisotropy values of the probe DPH embedded in a PGCL liposome were evaluated at two different temperatures, 25 °C and 50 °C, to ensure its sensitivity to the molecular liposomal environment. As the temperature increases, the bilayer should become more fluid, and anisotropy should decrease. Initially, a molar probe:lipid ratio of 1:800 was used and added after liposome extrusion, but this led to overwhelmingly high intensity signals. At high DPH concentrations, the anisotropy was extremely low, owing to the “drowning out” of the signal by the high fluorescence of DPH. Under these conditions, any changes in anisotropy are very small and difficult to quantify because the initial anisotropy signal is small. When the probe:lipid ratio was decreased to 1:30,000, the anisotropy increased significantly, but the probe still lacked any sensitivity to the molecular liposomal environment, as seen in the minimal difference between the anisotropy signal at 25 °C and 50 °C. Finally, the probe:lipid ratio was decreased further to 1:50,000 and the DPH probe was preferentially embedded within the bilayer by drying down DPH onto the lipid film prior to re-hydration. This final condition led to not only high anisotropy signal (as compared to the initial condition) but also a dramatic difference in the signal at 25 °C and 50 °C, showing the sensitivity of the probe to the molecular liposomal environment under

these conditions (**Figure 7**). More work is required to fully optimize the conditions for the fluorescence anisotropy studies, but the sensitivity of the probe under these conditions was sufficient to study the differences in bilayer fluidity induced by AgNPs.

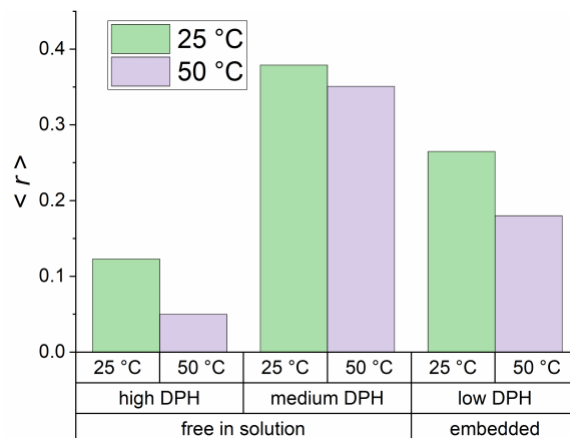


Figure 7. Optimization of DPH concentration and embedding method. From left to right, the molar probe:lipid ratios of the “high,” “medium,” and “low” DPH conditions correspond to 1:800, 1:20,000, and 1:50,000. Conditions marked “free in solution” represent samples where free DPH was added to liposomes after extrusion, whereas conditions marked “embedded” represent samples where DPH is dried down on top of the lipid film before re-hydration. The final condition was chosen for all future fluorescence anisotropy studies.

Chapter 5: Quantifying Time-Dependent Changes in the *C. crescentus* Phospholipid Bilayer Induced by AgNPs

5.1: The Eco-Corona Modulates AgNP Adhesion to the *C. crescentus* Bilayer

DLS time-resolved studies were conducted to probe how liposome size changes upon interaction with AgNPs. In this study, PGCL liposomes were incubated at 30 °C and every two hours for the first ten hours, their average size was measured, as well as a final measurement at 24 hours. As a control, first the PGCL liposome alone was measured over the 24-hour period, and no significant size changes were observed. Additionally, when the PGCL liposome was incubated with just dilute spent medium in the absence of AgNPs, no size changes were seen over 24 hours (**Table A2**). When the liposome was incubated with 2 mg L⁻¹ AgNPs, the diameter of the liposomes increased slightly. Note, only the peak corresponding to the liposomes, centered near 160 nm, was used to calculate the liposome diameter rather than the Z-ave peak since it could contain peaks attributed to the AgNPs and lower the average diameter. However, when the PGCL liposome was incubated with 2 mg L⁻¹ SM-AgNPs, two distinct behaviors were observed. First, over the initial 10 hours the average size of the liposomes slightly decreased. Then, after 24 hours of interaction, the size increased back to the original diameter, but the sample became less homogeneous and had a broader distribution (**Figure 8, Table A2**).

Additionally, the impact of AgNPs on sample heterogeneity is worth considering. After 2 hours, the PDI of the liposome control was 0.16 ± 0.02 , but this increased to 0.26 ± 0.07 in the liposomes incubated with AgNPs showing an increase in the polydispersity of the sample. However, it is important to remember that a significant factor in this heterogeneity is the presence of the bare AgNPs peak. After 2 hours, the liposomes

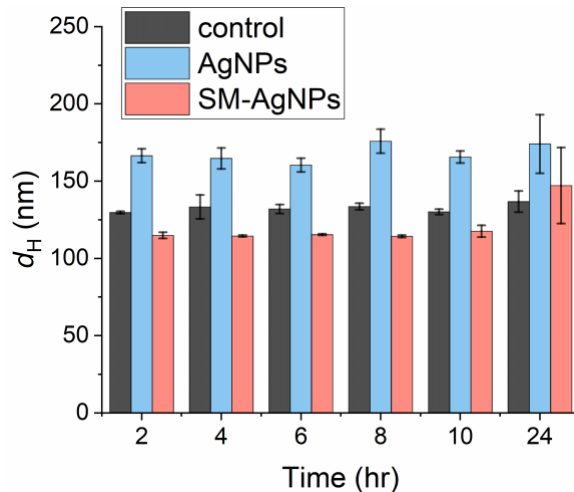


Figure 8. PGCL liposome hydrodynamic diameters over 24 hours at 30 °C. Average diameters of liposome controls, with 2 mg L⁻¹ AgNPs, and with 2 mg L⁻¹ SM-AgNPs. Note: the average size diameters for AgNP samples were taken from the average size of the first peak, not the Z-ave value. All measurements were run in triplicate.

incubated with SM-AgNPs had a PdI of 0.204 ± 0.002 , showing a slight increase in heterogeneity, but not to the level of the liposomes incubated with AgNPs. Over the 24-hour period, the liposomes with SM-AgNPs had a PdI similar to or lower than that seen for the liposome control, showing the stabilizing effect of the SM-AgNPs on the liposomes' tendency to agglomerate over time. After 24 hours, the liposome control had a PdI of 0.20 ± 0.04 , whereas the liposomes incubated with AgNPs had a PdI of 0.3 ± 0.1 and the liposomes incubated with SM-AgNPs had a PdI of 0.28 ± 0.06 , showing that the initial stabilizing effect seen by the SM-AgNPs is non-existent after 24 hours incubation (**Table A3**). Together, these results show that incubation with both types of AgNPs increased the heterogeneity of the liposome size over time, with bare AgNPs increasing their polydispersity at all time points studied and SM-AgNPs having the greatest effect only after a full 24 hours of incubation.

To understand the changes in average liposome diameter, the size distributions at each time point were analyzed. **Figure 9** shows the average size distributions from the triplicate samples of the control samples with both the AgNP and SM-AgNP liposome size distributions superimposed over the control distributions. The AgNP liposome size distributions show the presence of an AgNP peak around 20 nm (**Figure 9A**), which is absent in the SM-AgNP liposome size distributions. This indicates that the interaction between liposomes and AgNPs is weak, as a measurable amount of AgNPs are not adhered to the liposomes even after 24 hours of interaction. From these histograms, it can also be seen that bare AgNPs adhere to the surface of the liposomes, as there is a small but noticeable increase in the center of the liposomes' size distribution upon incubation with AgNPs at all time points (**Figure 9A**).

Over the first 10 hours of SM-AgNP interaction with liposomes, the center of the liposomes' size distribution is shifted to smaller diameters (**Figure 9B**). After 24 hours, the liposome size distribution greatly broadens and shifts to larger values (**Figure 9B**, final panel). The absence of a SM-AgNP peak suggests a possible encapsulation mechanism in which the average size of the liposome slightly decreases. The fluid nature of the bilayer could lend itself to distort inward as the SM-AgNP is encapsulated such that the diameter of the liposome appears smaller. Then, after 24 hours, it's possible that the distortion reverses, indicating the full internalization of the SM-AgNPs because the average size of the liposomes has been restored to its original value but with a notably broader size distribution. Alternatively, the initial decrease in liposome size upon incubation with SM-AgNPs could be due to lipid extraction, and the formation of a lipid corona around the SM-AgNPs. Then, the final increase in size and broadening in the size

distribution is possibly explained by the fusion of lipid-coated SM-AgNPs to the liposomes, creating large particles.

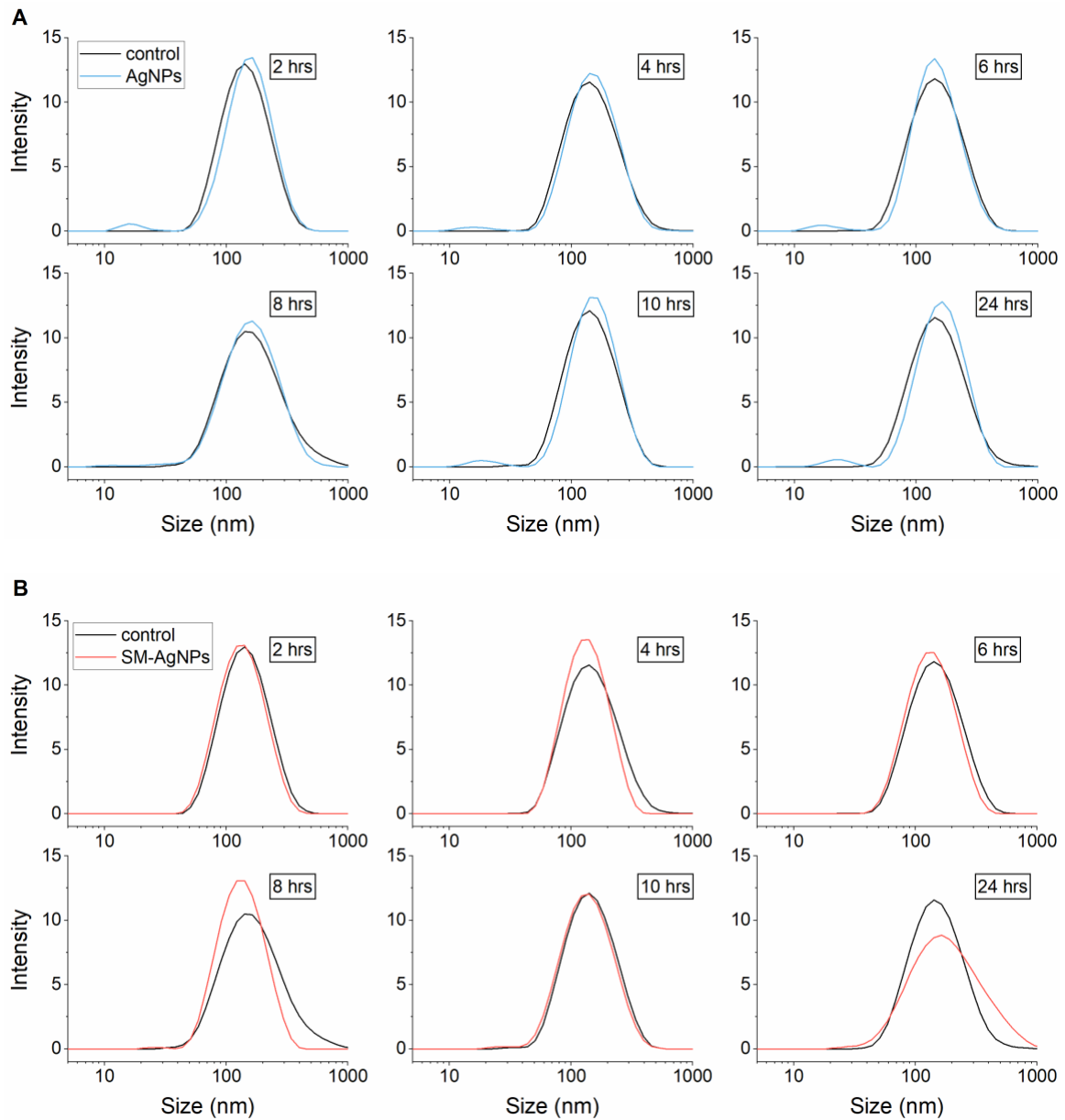


Figure 9. DLS histograms showing the averaged size distributions of PGCL liposomes (control) over 24 hours at 30 °C and the changes induced by (SM-)AgNPs. **(A)** Size distributions with 2 mg L⁻¹ AgNPs over 24 hours. **(B)** Size distributions with 2 mg L⁻¹ SM-AgNPs over 24 hours. All samples were run in triplicate.

5.2: AgNP Adhesion to the *C. crescentus* Bilayer Increases Membrane Rigidity

Time-resolved fluorescence anisotropy studies were conducted to probe how liposome membrane fluidity changes upon interaction with AgNPs. In this study, PGCL liposomes were incubated in 30 °C and every two hours for the first ten hours, their anisotropy was measured, as well as a final 24-hour measurement. The anisotropy parameter is directly related to the fluidity of the bilayer. Lower anisotropy values indicate facile mobility of the DPH probe and thus a more fluid bilayer whereas higher anisotropy values indicate limited DPH probe mobility and a more rigid bilayer. Based on changes to the normal fluidity of the bilayer, disturbances to the order of the phospholipids induced by AgNPs can be inferred.

Over the first 10 hours, the liposome control naturally increased in rigidity (**Figure 10A**). This is likely due to storage at 30 °C instead of normal storage conditions for the liposomes at 4 °C which maintain membrane stability. The addition of AgNPs to the liposome further increased this effect, with AgNPs consistently decreasing membrane fluidity compared to the liposome control at 2, 4, 6, 8, and 10 hours. In contrast, SM-AgNP samples had no difference in anisotropy from the control liposome samples (**Figure 10A**). This suggests that the bare AgNPs initially have a more disruptive interaction with the bilayer, inducing order and preventing the full fluidity of the membrane. This result agrees with the DLS size results, where AgNP adhesion to the surface of the liposome can pull phospholipids out of the natural order of the membrane into contact with the AgNP to reduce the cost of adhesion.

After 24 hours, however, this trend is almost entirely reversed. At 24 hours, the control sample has the highest rigidity, followed by the AgNP sample and finally the SM-

AgNP sample with the highest fluidity of the three (**Figure 10B**). At the 24 hour time point, the anisotropy of the AgNP sample is not significantly lower than the control sample ($p > 0.1$), but the SM-AgNPs sample is significantly lower ($p < 0.01$). At 24 hours, the AgNP liposome interaction has reached a steady state, in which the fluidity of the bilayer is no longer significantly affected by the presence of AgNPs adhered to the surface.

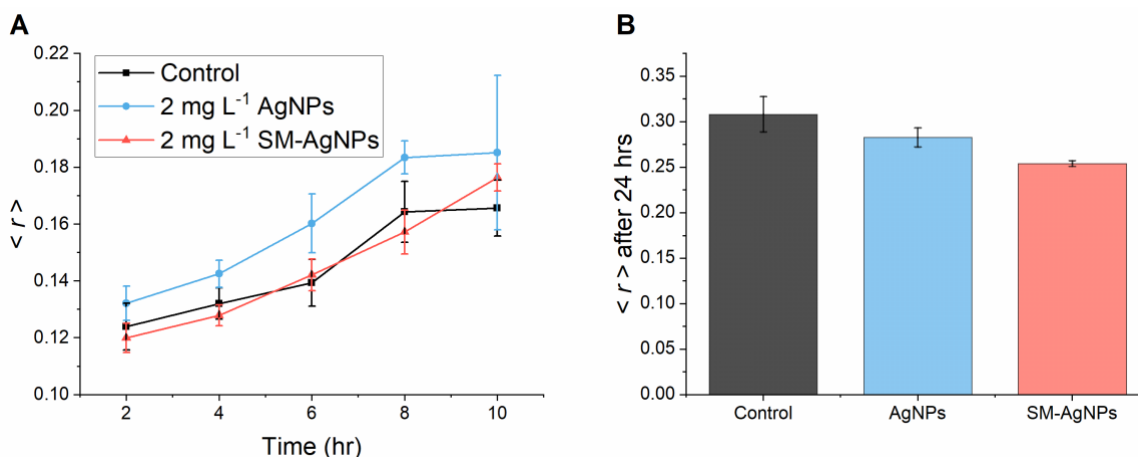


Figure 10. Anisotropy, $\langle r \rangle$, of DPH-embedded PGCL liposomes over 24 hours at 30 °C and the changes induced by (SM-) AgNPs. **(A)** Changes in anisotropy for the first 10 hours in control liposome samples, with 2 mg L⁻¹ AgNPs, and with 2 mg L⁻¹ SM-AgNPs. **(B)** Final anisotropy values after 24 hours incubation. All samples were run in triplicate.

The anisotropy results also support the partial encapsulation mechanism of the SM-AgNPs. Because of the eco-corona adsorbed to the AgNP surface, even when embedded within the phospholipid bilayer, it does not have significant effects on the orderliness of the membrane over the first ten hours of interaction. Over this time, the membrane is postulated to be distorted inward, and even with this distortion the lipids maintain the same degree of fluidity. However, when the SM-AgNP liposome interaction reaches a steady state after 24 hours, the inward distortion has been reversed and the

liposome has internalized the SM-AgNP. After this internalization, the membrane exhibits a higher degree of fluidity, indicating the full internalization and encapsulation of the SM-AgNPs. Various studies have similarly reported the interaction of a drug encapsulating within a liposome significantly affecting its fluidity, with most showing the increase in fluidity caused by interactions between the encapsulated drug and the phospholipid heads and/or tails, depending on which region the drug is encapsulated within.¹⁰⁸ Similarly, it is hypothesized that after being fully encapsulated, SM-AgNPs interact with phospholipids through their adsorbates and thereby increase fluidity of the bilayer.

Chapter 6: Conclusions and Future Directions

This work aimed to develop environmentally relevant *in vivo* and *in vitro* model systems to probe the interaction of AgNPs with the phospholipid bilayer, and, to understand the modulatory effect of the eco-corona in this interaction. First, the antibacterial toxicity of AgNPs was probed using *C. crescentus in vivo* growth curves. These data showed that AgNPs slowed the growth of bacteria, and the addition of the eco-corona increased this effect and further led to a decrease in the maximum growth reached by the culture. These results suggest that the eco-corona enhances toxicity of AgNPs and directed future studies to understand this enhanced toxicity as a result of interactions with the cell membrane.

Next, the work sought to develop a relevant *in vitro* model system based on the membrane composition of *C. crescentus* to probe interactions of AgNPs and SM-AgNPs with the phospholipid bilayer. Using DLS to probe the size changes of liposomes upon incubation with nanoparticles, it was found that bare AgNPs cause small increases in the size of the liposomes while many AgNPs remained free and unbound to the membrane. On the other hand, SM-AgNPs cause small decreases in the size of the liposomes and no observable SM-AgNP peak, likely due to particle aggregation. Together, these data suggest the differential interactions of AgNPs and SM-AgNPs with the phospholipid bilayer.

To further probe these suggested mechanisms, fluorescence anisotropy was used to study changes in membrane fluidity and rigidity induced by nanoparticles. Compared to the control, AgNPs increased the rigidity initially but then this effect fell off and the control samples had the same order as the AgNP-liposome samples. Conversely, SM-

AgNPs had no impact on the fluidity of the membrane initially but eventually increased the fluidity of the membrane. Together, these data further support the differential reactivities of AgNPs and SM-AgNPs with phospholipid bilayers.

Based on these results, the suggested mechanism of AgNP interaction is adhesion and SM-AgNP interaction is encapsulation and/or lipid extraction. AgNP weak adhesion to the bilayer disturbs the order of the phospholipids, increases the rigidity of the membrane, and increases the liposome size. This effect falls off as the AgNP reaches a steady state in its interaction with the liposome, as the order of the liposome and its size are restored (**Figure 11A**). Based on these methods alone, it is impossible to fully deduce whether SM-AgNPs interact with the phospholipid membrane through encapsulation or lipid extraction. Further work is needed to differentiate between these mechanisms. If SM-AgNPs interact via encapsulation, due to their coating of biomolecular adsorbates they have little effect on the fluidity of the membrane and can preferentially segregate to the interior of the membrane, slightly decreasing the liposome size. Eventually, these SM-AgNPs become fully encapsulated, and increase membrane fluidity from within the liposomes while restoring liposome size (**Figure 11B**). Alternatively, if SM-AgNPs interact via lipid extraction, they initially withdraw some lipids from the bilayer, decreasing the size of the liposome while having little effect on membrane fluidity. Eventually, these lipid-coated SM-AgNPs re-fuse with the liposomes, creating larger heteroaggregates with a high fluidity due to this fusion of the bilayers (**Figure 11C**).

It is important to recognize several limitations of the liposomal model system in contextualizing the *in vivo* results. While the liposomes exactly mimicked the phospholipid composition of the *C. crescentus* cell membrane, the more complex

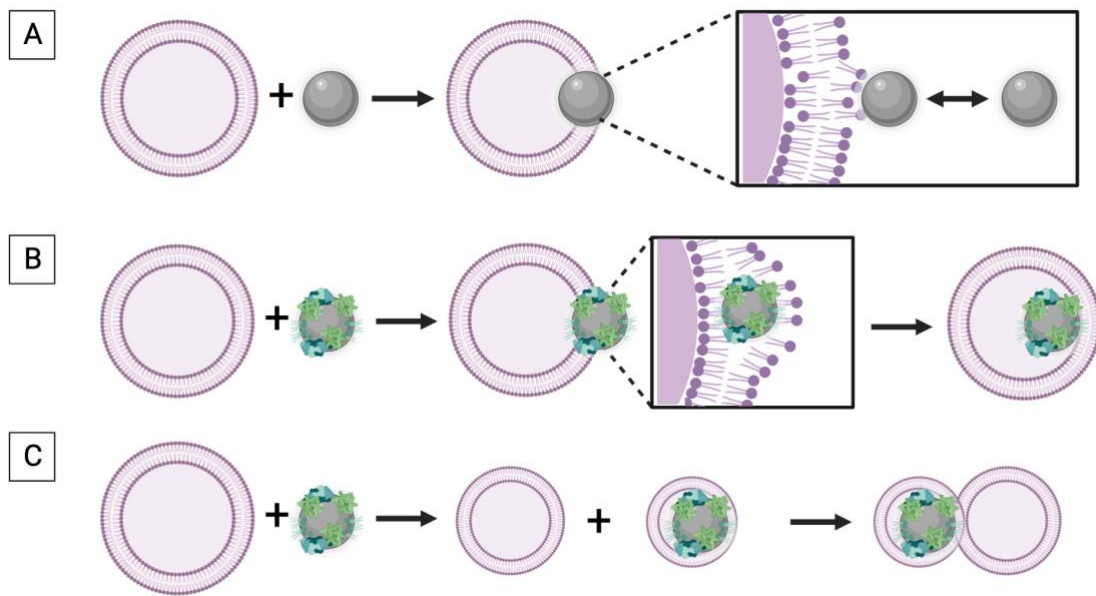


Figure 11. Proposed mechanism of interaction of AgNPs with phospholipid bilayers. **(A)** Bare AgNPs weakly adhere to the outside of the bilayer, causing a slight size increase and changing the orderliness of the membrane. **(B)** SM-AgNPs preferentially embed within the bilayer, causing minimal size changes and not disrupting the order of the membrane. **(C)** Alternatively, SM-AgNPs extract lipids from the membrane before eventually fusing to the liposomes. Created with Biorender.com

membrane components such as transmembrane proteins and the S-layer were not modeled in this study. Additionally, the liposomes used in this work were LUVs, which as discussed earlier have a vastly different curvature and size from a cell, which can in turn have a large impact on the interactions between these model membranes and AgNPs. Finally, the enhanced interaction of SM-AgNPs with *C. crescentus* and the model membranes are likely driven by different forces. Due to molecular recognition, SM-AgNPs may have enhanced uptake and toxicity to *C. crescentus* that is not seen in the model membrane studies, which simply model electrostatic effects. As useful as the liposomal model system is in developing potential mechanisms of toxicity, it is crucial to

recognize the key differences between living organisms and liposomes in order to fully understand the different reactivities observed in this study.

The complex eco-corona made up of the components of the spent medium of *C. crescentus* significantly modulates the manner in which AgNPs impact the growth of *C. crescentus*. This eco-corona is made up of proteins, lipids, and metabolites that all can adsorb to the AgNP surface, affecting its behavior and interactions. To further understand the manner in which SM-AgNPs modulate AgNP antibacterial toxicity, the effect of each eco-corona component should be studied individually and in different combinations. Through these studies, the exact function of the eco-corona could be elucidated in a piece-wise manner, allowing for enhanced prediction in a variety of environments.

Moreover, studies in addition to the *in vivo* growth study should be completed in order to better understand antibacterial toxicity of AgNPs. There are many common bacterial toxicity assays available commercially that can assess toxicity indicators such as respiration, ROS generation, and dehydrogenase activity. Additionally, the viability of a culture can be assessed over a longer time period than the 9 hours in this study using a fluorescence microplate viability assay. As this research expands, more sensitive toxicity assays than the *in vivo* growth study will be needed to accurately and sensitively probe AgNP antibacterial activity. Finally, the role of dissolved $\text{Ag(I)}_{(aq)}$ needs to be understood in bacterial studies. As effective as the liposome model membrane system is, it is limited in that it cannot capture the antibacterial toxicity of $\text{Ag(I)}_{(aq)}$. Thus, representative dissolution studies must be conducted in order to understand how much of the observed adverse effects in this work are due to physical AgNP interactions, and how much can be attributed to the effects of $\text{Ag(I)}_{(aq)}$.

The methods explored in detail above represent only a small sampling of the available techniques currently used to study the nanoparticle-bilayer interface. Future directions of this study should explore other analytical methods to understand AgNP-membrane interactions and further support the suggested mechanism. Time-dependent leakage of fluorescent dye from liposomes as a function of nanoparticle can be used to measure pore formation and permeability changes induced by AgNP adhesion to the bilayer.^{65,66} Future work should include development of fluorescent dye leakage methods, as this can directly probe AgNP adhesion and lipid extraction. In this method, both AgNPs and SM-AgNPs would be expected to generate leakage but due to their differential interactions, AgNPs should cause consistent pore formation whereas SM-AgNPs would induce pore formation initially but then effect would decrease over time as the SM-AgNPs were fully encapsulated or fused back onto the liposomes.

Various electrochemical techniques have also been developed, mainly using SLBs directly attached to an electrode. These studies can then be used to measure conductance of the bilayer and pore formation allowing leakage of contents and creating an ion current due to interaction of AgNPs.¹⁰⁹ SLBs can also be used in QCM-D studies which provide insight into single particle deformations, phase changes, and adhesion.¹¹⁰ Studies using electrochemistry and/or QCM-D are of utmost importance to continue the work on this project, as they will directly probe adhesion of the AgNPs. The suggested mechanism of this work hypothesizes that AgNPs will dynamically exchange with the bilayer, and through QCM-D this could be easily visualized through the loss and gain off adhered mass. Additionally, QCM-D could be powerfully used to probe the mechanism of SM-

AgNP interaction with bilayers, by showing a consistent increase in mass, showing the stronger adhesion to the membrane eventually leading to encapsulation.

Finally, in this current work only one membrane composition was tested, 9:1 PG to CL, based on the membrane composition of *C. crescentus*. Future work should explore alternate membrane compositions to probe the role of electrostatics in AgNP-membrane interactions. Both AgNPs and PGCL liposomes are strongly negatively charged, leading to an initial repulsion that makes any interaction more costly. However, if the phospholipid phosphatidylcholine (PC) were used in place of PG, this electrostatic repulsion could be reduced. Instead of an anionic head group like PG, PC has a zwitterionic head group, thereby reducing electrostatic repulsions.

Beyond studying specific AgNP-membrane interactions, this research can be applied to a wider understanding of AgNP antibacterial toxicity. Through this study, a simple, environmentally relevant eco-corona was seen to enhance AgNP toxicity. More work needs to be done to understand the complex factors that control this interaction, but it is important to recognize that studies on bare AgNPs alone ignore a larger picture understanding of the pathways through which AgNPs end up in the environment. Especially with the enhanced toxicity seen in this work, it is critical to continue enriching the scientific community's understanding of the environmental impacts of coronated AgNPs and their antibacterial activity.

Acknowledgments

I have far too many people that I need to acknowledge and thank for all their help and support over the length of this project. First, I need to thank the members of the Riley Lab, starting with my advisor, Dr. Kathryn Riley. You were instrumental at every step of writing this thesis, as well as my journey throughout Swarthmore. You were the first person who inspired me to go into chemistry, and I am so grateful for all life advice, scientific guidance, and excellent lab dinners you have provided along the way. I cannot thank you enough. Next, I would like to thank my great friends within the Riley Lab, starting with Chris Chung for putting up with me from the very start; Tim Kihiczak for his help with the bacterial aspect of this project; Casey Jordan, Michael Caprise, and Mary Garcia-Barrios for putting together an awe-inspiring lab culture over the summer; and Tyler Hicks for their help in running some of these time-based experiments. Thank you all, and I will miss you guys so much next year!

I would also like to thank all of my funding sources for the opportunity to conduct this research and the Swarthmore College Chemistry Department for allowing me to conduct this research. I would specifically like to thank Drs. Kathleen Howard and Amy Vollmer for their help in designing the model membrane system used in this work.

Finally, I would like to thank my family and friends outside of the Riley Lab for their support: I couldn't have done this alone. It is because of all of you that I am where I am, and I am so grateful for all of your continued interest in my work and encouragement over the many years. As much as this thesis was written through many hours in the lab, my sanity was saved with Film Fridays, Sharples meals, runs with the track team, and drinking tea with friends. Thank you all!

Appendix

Table A1. Optical densities of *C. crescentus* for the *in vivo* growth curve study.

Time (hr)	Optical density ^a (OD ₆₀₀)		
	Control	AgNPs	SM-AgNPs
0	0.20 ± 0.02	0.15 ± 0.06	0.13 ± 0.01
0.5	0.22 ± 0.02	0.19 ± 0.02	0.15 ± 0.01
1	0.28 ± 0.02	0.25 ± 0.01	0.18 ± 0.01
1.5	0.35 ± 0.03	0.31 ± 0.02	0.26 ± 0.02
2	0.43 ± 0.02	0.37 ± 0.02	0.34 ± 0.03
2.5	0.52 ± 0.04	0.47 ± 0.03	0.41 ± 0.03
3	0.64 ± 0.01	0.58 ± 0.04	0.57 ± 0.03
3.5	0.79 ± 0.03	0.69 ± 0.04	0.66 ± 0.04
4	0.88 ± 0.05	0.81 ± 0.06	
4.5	0.96 ± 0.03	0.90 ± 0.01	0.82 ± 0.04
5	1.03 ± 0.03	0.98 ± 0.03	0.92 ± 0.02
5.5	1.09 ± 0.03	1.03 ± 0.03	
7			1.05 ± 0.03
8		1.17 ± 0.02	

^aAll cultures were grown in triplicate. The absorbance of solutions of (SM-) AgNPs alone in PYE was used for baseline correction of the AgNP and SM-AgNP cultures.

Table A2. Liposome hydrodynamic diameters obtained through DLS.

Time (hr)	Hydrodynamic diameter of liposome ^a (nm)			
	Control	AgNPs	SM-AgNPs	Control + SM
2	129.7 ± 0.8	132 ± 3	115 ± 2	
4	133 ± 8	126 ± 3	114.5 ± 0.6	
6	132 ± 3	133 ± 5	115.4 ± 0.5	
8	134 ± 2	133.0 ± 0.2	114.3 ± 0.8	
10	130 ± 2	131 ± 4	118 ± 4	
24	137 ± 7	136 ± 7	150 ± 20	133 ± 3

^aAll samples were incubated and analyzed at 30 °C and run in triplicate.

Table A3. Liposome polydispersity indices obtained through DLS.

Time (hr)	Polydispersity index of liposome^a			
	Control	AgNPs	SM-AgNPs	Control + SM
2	0.16 ± 0.02	0.26 ± 0.07	0.204 ± 0.002	
4	0.19 ± 0.05	0.3 ± 0.1	0.195 ± 0.003	
6	0.18 ± 0.02	0.27 ± 0.08	0.203 ± 0.009	
8	0.21 ± 0.07	0.3 ± 0.1	0.197 ± 0.003	
10	0.18 ± 0.01	0.26 ± 0.08	0.21 ± 0.02	
24	0.20 ± 0.04	0.3 ± 0.1	0.28 ± 0.06	0.16 ± 0.03

^aAll samples were incubated and analyzed at 30 °C and run in triplicate.

References

- (1) Vance, M. E.; Kuiken, T.; Vejerano, E. P.; McGinnis, S. P.; Hochella, M. F.; Rejeski, D.; Hull, M. S. Nanotechnology in the Real World: Redeveloping the Nanomaterial Consumer Products Inventory. *Beilstein J. Nanotechnol.* **2015**, *6*, 1769–1780. <https://doi.org/10.3762/bjnano.6.181>.
- (2) Pulit-Prociak, J.; Banach, M. Silver Nanoparticles – a Material of the Future...? *Open Chemistry* **2016**, *14* (1), 76–91. <https://doi.org/10.1515/chem-2016-0005>.
- (3) Calderón-Jiménez, B.; Johnson, M. E.; Montoro Bustos, A. R.; Murphy, K. E.; Winchester, M. R.; Vega Baudrit, J. R. Silver Nanoparticles: Technological Advances, Societal Impacts, and Metrological Challenges. *Front. Chem.* **2017**, *5*. <https://doi.org/10.3389/fchem.2017.00006>.
- (4) Chen, S. F.; Zhang, H. Aggregation and Dissolution Kinetics of Nanosilver in Seawater. *Asian J. Chem.* **2013**, *25* (5), 2886–2888. <https://doi.org/10.14233/ajchem.2013.14380>.
- (5) Béltéky, P.; Rónavári, A.; Igaz, N.; Szerencsés, B.; Tóth, I. Y.; Pfeiffer, I.; Kiricsi, M.; Kónya, Z. Silver Nanoparticles: Aggregation Behavior in Biorelevant Conditions and Its Impact on Biological Activity. *IJN* **2019**, *Volume 14*, 667–687. <https://doi.org/10.2147/IJN.S185965>.
- (6) Li, X.; Lenhart, J. J.; Walker, H. W. Aggregation Kinetics and Dissolution of Coated Silver Nanoparticles. *Langmuir* **2012**, *28* (2), 1095–1104. <https://doi.org/10.1021/la202328n>.
- (7) Azodi, M.; Sultan, Y.; Ghoshal, S. Dissolution Behavior of Silver Nanoparticles and Formation of Secondary Silver Nanoparticles in Municipal Wastewater by Single-Particle ICP-MS. *Environmental Science & Technology* **2016**, *50* (24), 13318–13327. <https://doi.org/10.1021/acs.est.6b03957>.
- (8) Yan, N.; Xie, S.; Tang, B. Z.; Wang, W.-X. Real-Time Monitoring of the Dissolution Kinetics of Silver Nanoparticles and Nanowires in Aquatic Environments Using an Aggregation-Induced Emission Fluorogen. *Chemical Communications* **2018**, *54* (36), 4585–4588. <https://doi.org/10.1039/C8CC02245C>.
- (9) Yang, Y.; Zheng, S.; Li, R.; Chen, X.; Wang, K.; Sun, B.; Zhang, Y.; Zhu, L. New Insights into the Facilitated Dissolution and Sulfidation of Silver Nanoparticles under Simulated Sunlight Irradiation in Aquatic Environments by Extracellular Polymeric Substances. *Environ. Sci.: Nano* **2021**, *8* (3), 748–757. <https://doi.org/10.1039/D0EN01142H>.
- (10) Durán, N.; Silveira, C. P.; Durán, M.; Martinez, D. S. T. Silver Nanoparticle Protein Corona and Toxicity: A Mini-Review. *J Nanobiotechnology* **2015**, *13*. <https://doi.org/10.1186/s12951-015-0114-4>.
- (11) Argentiere, S.; Cella, C.; Cesaria, M.; Milani, P.; Lenardi, C. Silver Nanoparticles in Complex Biological Media: Assessment of Colloidal Stability and Protein Corona Formation. *Journal of Nanoparticle Research* **2016**, *18* (8). <https://doi.org/10.1007/s11051-016-3560-5>.
- (12) Levard, C.; Hotze, E. M.; Lowry, G. V.; Brown, G. E. Environmental Transformations of Silver Nanoparticles: Impact on Stability and Toxicity.

- Environ. Sci. Technol.* **2012**, *46* (13), 6900–6914.
<https://doi.org/10.1021/es2037405>.
- (13) Fadare, O. O.; Wan, B.; Liu, K.; Yang, Y.; Zhao, L.; Guo, L.-H. Eco-Corona vs Protein Corona: Effects of Humic Substances on Corona Formation and Nanoplastic Particle Toxicity in *Daphnia Magna*. *Environ. Sci. Technol.* **2020**, *54* (13), 8001–8009. <https://doi.org/10.1021/acs.est.0c00615>.
- (14) Wheeler, K. E.; Chetwynd, A. J.; Fahy, K. M.; Hong, B. S.; Tochihiuti, J. A.; Foster, L. A.; Lynch, I. Environmental Dimensions of the Protein Corona. *Nat. Nanotechnol.* **2021**, *16* (6), 617–629. <https://doi.org/10.1038/s41565-021-00924-1>.
- (15) Westmeier, D.; Stauber, R. H.; Docter, D. The Concept of Bio-Corona in Modulating the Toxicity of Engineered Nanomaterials (ENM). *Toxicology and Applied Pharmacology* **2016**, *299*, 53–57.
<https://doi.org/10.1016/j.taap.2015.11.008>.
- (16) Morsella, M.; d’Alessandro, N.; Lanterna, A. E.; Scaiano, J. C. Improving the Sunscreen Properties of TiO₂ through an Understanding of Its Catalytic Properties. *ACS Omega* **2016**, *1* (3), 464–469.
<https://doi.org/10.1021/acsomega.6b00177>.
- (17) Bakry, R.; Vallant, R. M.; Najam-ul-Haq, M.; Rainer, M.; Szabo, Z.; Huck, C. W.; Bonn, G. K. Medicinal Applications of Fullerenes. *Int J Nanomedicine* **2007**, *2* (4), 639–649.
- (18) Bala Subramaniyan, S.; Veerappan, A. Water Soluble Cadmium Selenide Quantum Dots for Ultrasensitive Detection of Organic, Inorganic and Elemental Mercury in Biological Fluids and Live Cells. *RSC Adv.* **2019**, *9* (39), 22274–22281. <https://doi.org/10.1039/C9RA04753K>.
- (19) Su, Y.; Ashworth, V. E. T. M.; Geitner, N. K.; Wiesner, M. R.; Ginnan, N.; Rolshausen, P.; Roper, C.; Jassby, D. Delivery, Fate, and Mobility of Silver Nanoparticles in Citrus Trees. *ACS Nano* **2020**, *14* (3), 2966–2981.
<https://doi.org/10.1021/acsnano.9b07733>.
- (20) Contado, C. Nanomaterials in Consumer Products: A Challenging Analytical Problem. *Front. Chem.* **2015**, *3*. <https://doi.org/10.3389/fchem.2015.00048>.
- (21) Zahoor, M.; Nazir, N.; Iftikhar, M.; Naz, S.; Zekker, I.; Burlakovs, J.; Uddin, F.; Kamran, A. W.; Kallistova, A.; Pimenov, N.; Ali Khan, F. A Review on Silver Nanoparticles: Classification, Various Methods of Synthesis, and Their Potential Roles in Biomedical Applications and Water Treatment. *Water* **2021**, *13* (16), 2216. <https://doi.org/10.3390/w13162216>.
- (22) Shao, J.; Wang, B.; Li, J.; Jansen, J. A.; Walboomers, X. F.; Yang, F. Antibacterial Effect and Wound Healing Ability of Silver Nanoparticles Incorporation into Chitosan-Based Nanofibrous Membranes. *Materials Science and Engineering: C* **2019**, *98*, 1053–1063.
<https://doi.org/10.1016/j.msec.2019.01.073>.
- (23) Paladini, F.; Pollini, M. Antimicrobial Silver Nanoparticles for Wound Healing Application: Progress and Future Trends. *Materials (Basel)* **2019**, *12* (16), 2540.
<https://doi.org/10.3390/ma12162540>.

- (24) Konop, M.; Damps, T.; Misicka, A.; Rudnicka, L. Certain Aspects of Silver and Silver Nanoparticles in Wound Care: A Minireview. *Journal of Nanomaterials* **2016**, *2016*, 1–10. <https://doi.org/10.1155/2016/7614753>.
- (25) Rigo, C.; Roman, M.; Munivrana, I.; Vindigni, V.; Azzena, B.; Barbante, C.; Cairns, W. R. L. Characterization and Evaluation of Silver Release from Four Different Dressings Used in Burns Care. *Burns* **2012**, *38* (8), 1131–1142. <https://doi.org/10.1016/j.burns.2012.06.013>.
- (26) Kulthong, K.; Srisung, S.; Boonpavanitchakul, K.; Kangwansupamonkon, W.; Maniratanachote, R. Determination of Silver Nanoparticle Release from Antibacterial Fabrics into Artificial Sweat. *Particle and Fibre Toxicology* **2010**, *7* (1), 8. <https://doi.org/10.1186/1743-8977-7-8>.
- (27) Venkova, T.; Yeo, C. C.; Espinosa, M. Editorial: The Good, The Bad, and The Ugly: Multiple Roles of Bacteria in Human Life. *Front. Microbiol.* **2018**, *9*, 1702. <https://doi.org/10.3389/fmicb.2018.01702>.
- (28) Valdes, A. M.; Walter, J.; Segal, E.; Spector, T. D. Role of the Gut Microbiota in Nutrition and Health. *BMJ* **2018**, k2179. <https://doi.org/10.1136/bmj.k2179>.
- (29) Riemann, B. Potential Importance of Fish Predation and Zooplankton Grazing on Natural Populations of Freshwater Bacteriat. *APPL. ENVIRON. MICROBIOL.* **1985**, *50*, 7.
- (30) Taylor, P. G.; Townsend, A. R. Stoichiometric Control of Organic Carbon–Nitrate Relationships from Soils to the Sea. *Nature* **2010**, *464* (7292), 1178–1181. <https://doi.org/10.1038/nature08985>.
- (31) Lee, C. S.; Kim, M.; Lee, C.; Yu, Z.; Lee, J. The Microbiota of Recreational Freshwaters and the Implications for Environmental and Public Health. *Front. Microbiol.* **2016**, *7*. <https://doi.org/10.3389/fmicb.2016.01826>.
- (32) Byrd, A. L.; Belkaid, Y.; Segre, J. A. The Human Skin Microbiome. *Nat Rev Microbiol* **2018**, *16* (3), 143–155. <https://doi.org/10.1038/nrmicro.2017.157>.
- (33) Hayat, R.; Ali, S.; Amara, U.; Khalid, R.; Ahmed, I. Soil Beneficial Bacteria and Their Role in Plant Growth Promotion: A Review. *Ann Microbiol* **2010**, *60* (4), 579–598. <https://doi.org/10.1007/s13213-010-0117-1>.
- (34) Zhang, W. Nanoparticle Aggregation: Principles and Modeling. In *Nanomaterials*; Capco, D. G., Chen, Y., Eds.; Springer Netherlands: Dordrecht, 2014; Vol. 811, pp 19–43. https://doi.org/10.1007/978-94-017-8739-0_2.
- (35) Le Ouay, B.; Stellacci, F. Antibacterial Activity of Silver Nanoparticles: A Surface Science Insight. *Nano Today* **2015**, *10* (3), 339–354. <https://doi.org/10.1016/j.nantod.2015.04.002>.
- (36) Sondi, I.; Salopek-Sondi, B. Silver Nanoparticles as Antimicrobial Agent: A Case Study on E. Coli as a Model for Gram-Negative Bacteria. *Journal of Colloid and Interface Science* **2004**, *275* (1), 177–182. <https://doi.org/10.1016/j.jcis.2004.02.012>.
- (37) Manukumar, H. M.; Chandrasekhar, B.; Rakesh, K. P.; Ananda, A. P.; Nandhini, M.; Lalitha, P.; Sumathi, S.; Qin, H.-L.; Umesha, S. Novel T-C@AgNPs Mediated Biocidal Mechanism against Biofilm Associated Methicillin-Resistant *Staphylococcus Aureus* (Bap-MRSA) 090, Cytotoxicity and Its Molecular

- Docking Studies. *Med. Chem. Commun.* **2017**, *8* (12), 2181–2194. <https://doi.org/10.1039/C7MD00486A>.
- (38) Losasso, C.; Belluco, S.; Cibir, V.; Zavagnin, P.; MiÄ• etiÄ‡, I.; Gallochio, F.; Zanella, M.; Bregoli, L.; Biancotto, G.; Ricci, A. Antibacterial Activity of Silver Nanoparticles: Sensitivity of Different Salmonella Serovars. *Front. Microbiol.* **2014**, *5*. <https://doi.org/10.3389/fmicb.2014.00227>.
- (39) Liu, C.; Leng, W.; Vikesland, P. J. Controlled Evaluation of the Impacts of Surface Coatings on Silver Nanoparticle Dissolution Rates. *Environmental Science & Technology* **2018**, *52* (5), 2726–2734. <https://doi.org/10.1021/acs.est.7b05622>.
- (40) Wang, X.; Herting, G.; Odnevall Wallinder, I.; Blomberg, E. Adsorption of Bovine Serum Albumin on Silver Surfaces Enhances the Release of Silver at PH Neutral Conditions. *Physical Chemistry Chemical Physics* **2015**, *17* (28), 18524–18534. <https://doi.org/10.1039/C5CP02306H>.
- (41) Martin, M. N.; Allen, A. J.; MacCuspie, R. I.; Hackley, V. A. Dissolution, Agglomerate Morphology, and Stability Limits of Protein-Coated Silver Nanoparticles. *Langmuir* **2014**, *30* (38), 11442–11452. <https://doi.org/10.1021/la502973z>.
- (42) Ostermeyer, A.-K.; Kostigen Mumuper, C.; Semprini, L.; Radniecki, T. Influence of Bovine Serum Albumin and Alginate on Silver Nanoparticle Dissolution and Toxicity to Nitrosomonas Europaea. *Environ. Sci. Technol.* **2013**, *47* (24), 14403–14410. <https://doi.org/10.1021/es4033106>.
- (43) Loza, K.; Diendorf, J.; Sengstock, C.; Ruiz-Gonzalez, L.; Gonzalez-Calbet, J. M.; Vallet-Regi, M.; Köller, M.; Epple, M. The Dissolution and Biological Effects of Silver Nanoparticles in Biological Media. *Journal of Materials Chemistry B* **2014**, *2* (12), 1634. <https://doi.org/10.1039/c3tb21569e>.
- (44) Boehmler, D. J.; O’Dell, Z. J.; Chung, C.; Riley, K. R. Bovine Serum Albumin Enhances Silver Nanoparticle Dissolution Kinetics in a Size- and Concentration-Dependent Manner. *Langmuir* **2020**, *36* (4), 1053–1061. <https://doi.org/10.1021/acs.langmuir.9b03251>.
- (45) Axson, J. L.; Stark, D. I.; Bondy, A. L.; Capracotta, S. S.; Maynard, A. D.; Philbert, M. A.; Bergin, I. L.; Ault, A. P. Rapid Kinetics of Size and PH-Dependent Dissolution and Aggregation of Silver Nanoparticles in Simulated Gastric Fluid. *The Journal of Physical Chemistry C* **2015**, *119* (35), 20632–20641. <https://doi.org/10.1021/acs.jpcc.5b03634>.
- (46) Hui, J.; O’Dell, Z. J.; Rao, A.; Riley, K. R. In Situ Quantification of Silver Nanoparticle Dissolution Kinetics in Simulated Sweat Using Linear Sweep Stripping Voltammetry. *Environmental Science & Technology* **2019**, *53* (22), 13117–13125. <https://doi.org/10.1021/acs.est.9b04151>.
- (47) Fernando, I.; Zhou, Y. Impact of PH on the Stability, Dissolution and Aggregation Kinetics of Silver Nanoparticles. *Chemosphere* **2019**, *216*, 297–305. <https://doi.org/10.1016/j.chemosphere.2018.10.122>.
- (48) Zhang, W.; Yao, Y.; Sullivan, N.; Chen, Y. Modeling the Primary Size Effects of Citrate-Coated Silver Nanoparticles on Their Ion Release Kinetics. *Environ. Sci. Technol.* **2011**, *45* (10), 4422–4428. <https://doi.org/10.1021/es104205a>.

- (49) Peretyazhko, T. S.; Zhang, Q.; Colvin, V. L. Size-Controlled Dissolution of Silver Nanoparticles at Neutral and Acidic PH Conditions: Kinetics and Size Changes. *Environ. Sci. Technol.* **2014**, *48* (20), 11954–11961. <https://doi.org/10.1021/es5023202>.
- (50) Jung, W. K.; Koo, H. C.; Kim, K. W.; Shin, S.; Kim, S. H.; Park, Y. H. Antibacterial Activity and Mechanism of Action of the Silver Ion in *Staphylococcus Aureus* and *Escherichia Coli*. *Appl Environ Microbiol* **2008**, *74* (7), 2171–2178. <https://doi.org/10.1128/AEM.02001-07>.
- (51) Carlson, C.; Hussain, S. M.; Schrand, A. M.; K. Braydich-Stolle, L.; Hess, K. L.; Jones, R. L.; Schlager, J. J. Unique Cellular Interaction of Silver Nanoparticles: Size-Dependent Generation of Reactive Oxygen Species. *J. Phys. Chem. B* **2008**, *112* (43), 13608–13619. <https://doi.org/10.1021/jp712087m>.
- (52) Yin, I. X.; Zhang, J.; Zhao, I. S.; Mei, M. L.; Li, Q.; Chu, C. H. The Antibacterial Mechanism of Silver Nanoparticles and Its Application in Dentistry. *IJN* **2020**, *Volume 15*, 2555–2562. <https://doi.org/10.2147/IJN.S246764>.
- (53) Bolea-Fernandez, E.; Balcaen, L.; Resano, M.; Vanhaecke, F. Overcoming Spectral Overlap via Inductively Coupled Plasma-Tandem Mass Spectrometry (ICP-MS/MS). A Tutorial Review. *J. Anal. At. Spectrom.* **2017**, *32* (9), 1660–1679. <https://doi.org/10.1039/C7JA00010C>.
- (54) Afshinnia, K.; Gibson, I.; Merrifield, R.; Baalousha, M. The Concentration-Dependent Aggregation of Ag NPs Induced by Cystine. *Science of The Total Environment* **2016**, *557–558*, 395–403. <https://doi.org/10.1016/j.scitotenv.2016.02.212>.
- (55) Wang, F.; Chen, Z.; Wang, Y.; Ma, C.; Bi, L.; Song, M.; Jiang, G. Silver Nanoparticles Induce Apoptosis in HepG2 Cells through Particle-Specific Effects on Mitochondria. *Environ. Sci. Technol.* **2022**. <https://doi.org/10.1021/acs.est.1c08246>.
- (56) Yan, N.; Wang, W.-X. Novel Imaging of Silver Nanoparticle Uptake by a Unicellular Alga and Trophic Transfer to *Daphnia Magna*. *Environ. Sci. Technol.* **2021**, *55* (8), 5143–5151. <https://doi.org/10.1021/acs.est.0c08588>.
- (57) Cooper, G.; Hausman, R. *The Cell: A Molecular Approach*, 6th ed.; Sinauer Associates, Inc., 2019.
- (58) Alberts, B. Membrane Structure. In *Molecular Biology of the Cell*; Garland Science: New York, 2002.
- (59) Farnoud, A. M.; Nazemidashtarjandi, S. Emerging Investigator Series: Interactions of Engineered Nanomaterials with the Cell Plasma Membrane; What Have We Learned from Membrane Models? *Environ. Sci.: Nano* **2019**, *6* (1), 13–40. <https://doi.org/10.1039/C8EN00514A>.
- (60) Warren, E. A. K.; Payne, C. K. Cellular Binding of Nanoparticles Disrupts the Membrane Potential. *RSC Adv.* **2015**, *5* (18), 13660–13666. <https://doi.org/10.1039/C4RA15727C>.
- (61) Melby, E. S.; Lohse, S. E.; Park, J. E.; Vartanian, A. M.; Putans, R. A.; Abbott, H. B.; Hamers, R. J.; Murphy, C. J.; Pedersen, J. A. Cascading Effects of Nanoparticle Coatings: Surface Functionalization Dictates the Assemblage of

- Complexed Proteins and Subsequent Interaction with Model Cell Membranes. *ACS Nano* **2017**, *11* (6), 5489–5499. <https://doi.org/10.1021/acsnano.7b00231>.
- (62) Melby, E. S.; Allen, C.; Foreman-Ortiz, I. U.; Caudill, E. R.; Kuech, T. R.; Vartanian, A. M.; Zhang, X.; Murphy, C. J.; Hernandez, R.; Pedersen, J. A. Peripheral Membrane Proteins Facilitate Nanoparticle Binding at Lipid Bilayer Interfaces. *Langmuir* **2018**, *34* (36), 10793–10805. <https://doi.org/10.1021/acs.langmuir.8b02060>.
- (63) Wang, Q.; Lim, M.; Liu, X.; Wang, Z.; Chen, K. L. Influence of Solution Chemistry and Soft Protein Coronas on the Interactions of Silver Nanoparticles with Model Biological Membranes. *Environmental Science & Technology* **2016**, *50* (5), 2301–2309. <https://doi.org/10.1021/acs.est.5b04694>.
- (64) Chen, K. L.; Bothun, G. D. Nanoparticles Meet Cell Membranes: Probing Nonspecific Interactions Using Model Membranes. *Environ. Sci. Technol.* **2014**, *48* (2), 873–880. <https://doi.org/10.1021/es403864v>.
- (65) Negoda, A.; Liu, Y.; Hou, W. C.; Corredor, C.; Moghadam, B. Y.; Musolff, C.; Li, n; Walker, W.; Westerhoff, P.; Mason, A. J.; Duxbury, P.; Posner, J. D.; Worden, R. M. Engineered Nanomaterial Interactions with Bilayer Lipid Membranes: Screening Platforms to Assess Nanoparticle Toxicity. *IJBNN* **2013**, *3* (1/2), 52. <https://doi.org/10.1504/IJBNN.2013.054512>.
- (66) Moghadam, B. Y.; Hou, W.-C.; Corredor, C.; Westerhoff, P.; Posner, J. D. Role of Nanoparticle Surface Functionality in the Disruption of Model Cell Membranes. *Langmuir* **2012**, *28* (47), 16318–16326. <https://doi.org/10.1021/la302654s>.
- (67) Nabika, H.; Unoura, K. Interaction between Nanoparticles and Cell Membrane. In *Surface Chemistry of Nanobiomaterials*; Elsevier, 2016; pp 231–263. <https://doi.org/10.1016/B978-0-323-42861-3.00008-X>.
- (68) Contini, C.; Schneemilch, M.; Gaisford, S.; Quirke, N. Nanoparticle–Membrane Interactions. *Journal of Experimental Nanoscience* **2018**, *13* (1), 62–81. <https://doi.org/10.1080/17458080.2017.1413253>.
- (69) Park, S.-H.; Oh, S.-G.; Mun, J.-Y.; Han, S.-S. Effects of Silver Nanoparticles on the Fluidity of Bilayer in Phospholipid Liposome. *Colloids and Surfaces B: Biointerfaces* **2005**, *44* (2–3), 117–122. <https://doi.org/10.1016/j.colsurfb.2005.06.002>.
- (70) Bothun, G. D. Hydrophobic Silver Nanoparticles Trapped in Lipid Bilayers: Size Distribution, Bilayer Phase Behavior, and Optical Properties. *J Nanobiotechnol* **2008**, *6* (1), 13. <https://doi.org/10.1186/1477-3155-6-13>.
- (71) Zhang, X.; Pandiakumar, A. K.; Hamers, R. J.; Murphy, C. J. Quantification of Lipid Corona Formation on Colloidal Nanoparticles from Lipid Vesicles. *Anal. Chem.* **2018**, *90* (24), 14387–14394. <https://doi.org/10.1021/acs.analchem.8b03911>.
- (72) Wu, L.; Jiang, X. Recent Developments in Methodology Employed to Study the Interactions between Nanomaterials and Model Lipid Membranes. *Anal Bioanal Chem* **2016**, *408* (11), 2743–2758. <https://doi.org/10.1007/s00216-015-9157-5>.
- (73) Casci, T. It's a Bug's Life. *Nature Reviews Genetics*. 2001, p 84.

- (74) MacRae, J. D.; Smit, J. Characterization of Caulobacters Isolated from Wastewater Treatment Systems. *Appl Environ Microbiol* **1991**, *57* (3), 751–758. <https://doi.org/10.1128/aem.57.3.751-758.1991>.
- (75) Lorenz, C.; Windler, L.; von Goetz, N.; Lehmann, R. P.; Schuppler, M.; Hungerbühler, K.; Heuberger, M.; Nowack, B. Characterization of Silver Release from Commercially Available Functional (Nano)Textiles. *Chemosphere* **2012**, *89* (7), 817–824. <https://doi.org/10.1016/j.chemosphere.2012.04.063>.
- (76) Contreras, I.; Shapiro, L.; Henry, S. Membrane Phospholipid Composition of *Caulobacter Crescentus*. *J Bacteriol* **1978**, *135* (3), 1130–1136. <https://doi.org/10.1128/jb.135.3.1130-1136.1978>.
- (77) Hughes, V.; Jiang, C.; Brun, Y. *Caulobacter Crescentus*. *Current Biology* **2012**, *22* (13), R507–R509. <https://doi.org/10.1016/j.cub.2012.05.036>.
- (78) Prescott. Proteobacteria. In *Prescott's Microbiology*; 2017.
- (79) Govers, S. K.; Jacobs-Wagner, C. *Caulobacter Crescentus*: Model System Extraordinaire. *Current Biology* **2020**, *30* (19), R1151–R1158. <https://doi.org/10.1016/j.cub.2020.07.033>.
- (80) Chertkov, O.; Brown, P. J. B.; Kysela, D. T.; de Pedro, M. A.; Lucas, S.; Copeland, A.; Lapidus, A.; Del Rio, T. G.; Tice, H.; Bruce, D.; Goodwin, L.; Pitluck, S.; Detter, J. C.; Han, C.; Larimer, F.; Chang, Y.; Jeffries, C. D.; Land, M.; Hauser, L.; Kyrpides, N. C.; Ivanova, N.; Ovchinnikova, G.; Tindall, B. J.; Göker, M.; Klenk, H.-P.; Brun, Y. V. Complete Genome Sequence of *Hirschia Baltica* Type Strain (IFAM 1418T). *Stand. Genomic Sci.* **2011**, *5* (3), 287–297. <https://doi.org/10.4056/sigs.2205004>.
- (81) Prescott. Bacterial Cell Structure. In *Prescott's Microbiology*; 2017.
- (82) Levin, P. A.; Angert, E. R. Small but Mighty: Cell Size and Bacteria. *Cold Spring Harb Perspect Biol* **2015**, *7* (7), a019216. <https://doi.org/10.1101/cshperspect.a019216>.
- (83) Peetla, C.; Labhasetwar, V. Effect of Molecular Structure of Cationic Surfactants on Biophysical Interactions of Surfactant-Modified Nanoparticles with a Model Membrane and Cellular Uptake. *Langmuir* **2009**, *25* (4), 2369–2377. <https://doi.org/10.1021/la803361y>.
- (84) Peetla, C.; Jin, S.; Weimer, J.; Elegbede, A.; Labhasetwar, V. Biomechanics and Thermodynamics of Nanoparticle Interactions with Plasma and Endosomal Membrane Lipids in Cellular Uptake and Endosomal Escape. *Langmuir* **2014**, *30* (25), 7522–7532. <https://doi.org/10.1021/la5015219>.
- (85) Hong, S.; Leroueil, P. R.; Janus, E. K.; Peters, J. L.; Kober, M.-M.; Islam, M. T.; Orr, B. G.; Baker, J. R.; Banaszak Holl, M. M. Interaction of Polycationic Polymers with Supported Lipid Bilayers and Cells: Nanoscale Hole Formation and Enhanced Membrane Permeability. *Bioconjugate Chem.* **2006**, *17* (3), 728–734. <https://doi.org/10.1021/bc060077y>.
- (86) Kwak, K. J.; Valincius, G.; Liao, W.-C.; Hu, X.; Wen, X.; Lee, A.; Yu, B.; Vanderah, D. J.; Lu, W.; Lee, L. J. Formation and Finite Element Analysis of Tethered Bilayer Lipid Structures. *Langmuir* **2010**, *26* (23), 18199–18208. <https://doi.org/10.1021/la1021802>.

- (87) Frost, H.; Bond, T.; Sizmur, T.; Felipe-Sotelo, M. A Review of Microplastic Fibres: Generation, Transport, and Vectors for Metal(Loid)s in Terrestrial Environments. *Environ. Sci.: Processes Impacts* **2022**, *24* (4), 504–524. <https://doi.org/10.1039/D1EM00541C>.
- (88) Zhang, X.; Yang, S. Nonspecific Adsorption of Charged Quantum Dots on Supported Zwitterionic Lipid Bilayers: Real-Time Monitoring by Quartz Crystal Microbalance with Dissipation. *Langmuir* **2011**, *27* (6), 2528–2535. <https://doi.org/10.1021/la104449y>.
- (89) Wehbe, N.; Patra, D.; Abdel-Massih, R. M.; Baydoun, E. Modulation of Membrane Properties by Silver Nanoparticles Probed by Curcumin Embedded in 1,2-Dimyristoyl-Sn-Glycero-3-Phosphocholine Liposomes. *Colloids and Surfaces B: Biointerfaces* **2019**, *173*, 94–100. <https://doi.org/10.1016/j.colsurfb.2018.09.053>.
- (90) Park, M. V. D. Z.; Neigh, A. M.; Vermeulen, J. P.; de la Fonteyne, L. J. J.; Verharen, H. W.; Briedé, J. J.; van Loveren, H.; de Jong, W. H. The Effect of Particle Size on the Cytotoxicity, Inflammation, Developmental Toxicity and Genotoxicity of Silver Nanoparticles. *Biomaterials* **2011**, *32* (36), 9810–9817. <https://doi.org/10.1016/j.biomaterials.2011.08.085>.
- (91) Ault, A. P.; Stark, D. I.; Axson, J. L.; Keeney, J. N.; Maynard, A. D.; Bergin, I. L.; Philbert, M. A. Protein Corona-Induced Modification of Silver Nanoparticle Aggregation in Simulated Gastric Fluid. *Environ. Sci.: Nano* **2016**, *3* (6), 1510–1520. <https://doi.org/10.1039/C6EN00278A>.
- (92) Tai, J.-T.; Lai, C.-S.; Ho, H.-C.; Yeh, Y.-S.; Wang, H.-F.; Ho, R.-M.; Tsai, D.-H. Protein–Silver Nanoparticle Interactions to Colloidal Stability in Acidic Environments. *Langmuir* **2014**, *30* (43), 12755–12764. <https://doi.org/10.1021/la5033465>.
- (93) Yeo, E. L. L.; Azman, N. ‘Ain; Kah, J. C. Y. Stealthiness and Hematocompatibility of Gold Nanoparticles with Pre-Formed Protein Corona. *Langmuir* **2021**, *37* (16), 4913–4923. <https://doi.org/10.1021/acs.langmuir.1c00151>.
- (94) Limongi, T.; Canta, M.; Racca, L.; Ancona, A.; Tritta, S.; Vighetto, V.; Cauda, V. Improving Dispersal of Therapeutic Nanoparticles in the Human Body. *Nanomedicine* **2019**, *14* (7), 797–801. <https://doi.org/10.2217/nmm-2019-0070>.
- (95) Gunsolus, I. L.; Mousavi, M. P. S.; Hussein, K.; Bühlmann, P.; Haynes, C. L. Effects of Humic and Fulvic Acids on Silver Nanoparticle Stability, Dissolution, and Toxicity. *Environ. Sci. Technol.* **2015**, *49* (13), 8078–8086. <https://doi.org/10.1021/acs.est.5b01496>.
- (96) Brown, J.; Shannahan, J.; Podila, R. A Hyperspectral and Toxicological Analysis of Protein Corona Impact on Silver Nanoparticle Properties, Intracellular Modifications, and Macrophage Activation. *International Journal of Nanomedicine* **2015**, 6509. <https://doi.org/10.2147/IJN.S92570>.
- (97) Wang, X.; Fan, W.; Dong, Z.; Liang, D.; Zhou, T. Interactions of Natural Organic Matter on the Surface of PVP-Capped Silver Nanoparticle under Different Aqueous Environment. *Water Research* **2018**, *138*, 224–233. <https://doi.org/10.1016/j.watres.2018.03.048>.

- (98) Ritz, C. Toward a Unified Approach to Dose-Response Modeling in Ecotoxicology. *Environ Toxicol Chem* **2010**, 29 (1), 220–229. <https://doi.org/10.1002/etc.7>.
- (99) Chen, X. Liposome Characterization by DLS. *Wyatt Technology Corporation* **2005**.
- (100) Ramos, A. P. Dynamic Light Scattering Applied to Nanoparticle Characterization. In *Nanocharacterization Techniques*; Elsevier, 2017; pp 99–110. <https://doi.org/10.1016/B978-0-323-49778-7.00004-7>.
- (101) Stetefeld, J.; McKenna, S. A.; Patel, T. R. Dynamic Light Scattering: A Practical Guide and Applications in Biomedical Sciences. *Biophys Rev* **2016**, 8 (4), 409–427. <https://doi.org/10.1007/s12551-016-0218-6>.
- (102) Tomaszewska, E.; Soliwoda, K.; Kadziola, K.; Tkacz-Szczesna, B.; Celichowski, G.; Cichomski, M.; Szmaja, W.; Grobelny, J. Detection Limits of DLS and UV-Vis Spectroscopy in Characterization of Polydisperse Nanoparticles Colloids. *Journal of Nanomaterials* **2013**, 2013, 1–10. <https://doi.org/10.1155/2013/313081>.
- (103) Bhattacharjee, S. DLS and Zeta Potential – What They Are and What They Are Not? *Journal of Controlled Release* **2016**, 235, 337–351. <https://doi.org/10.1016/j.jconrel.2016.06.017>.
- (104) Malvern Panalytical, Inc. DLS and Zeta Potential Measurements; 2018.
- (105) Sepúlveda, B.; Angelomé, P. C.; Lechuga, L. M.; Liz-Marzán, L. M. LSPR-Based Nanobiosensors. *Nano Today* **2009**, 4 (3), 244–251. <https://doi.org/10.1016/j.nantod.2009.04.001>.
- (106) Sui, M.; Kunwar, S.; Pandey, P.; Lee, J. Strongly Confined Localized Surface Plasmon Resonance (LSPR) Bands of Pt, AgPt, AgAuPt Nanoparticles. *Sci Rep* **2019**, 9 (1), 16582. <https://doi.org/10.1038/s41598-019-53292-1>.
- (107) Park, S.-H.; Oh, S.-G.; Mun, J.-Y.; Han, S.-S. Effects of Silver Nanoparticles on the Fluidity of Bilayer in Phospholipid Liposome. *Colloids and Surfaces B: Biointerfaces* **2005**, 44 (2–3), 117–122. <https://doi.org/10.1016/j.colsurfb.2005.06.002>.
- (108) Zhao, J.; Mao, S. Tuning the Membrane Fluidity of Liposomes for Desirable in Vivo Fate with Enhanced Drug Delivery. In *Advances in Biomembranes and Lipid Self-Assembly*; Elsevier, 2021; Vol. 34, pp 67–106. <https://doi.org/10.1016/bs.abl.2021.11.003>.
- (109) Oh-hora, M.; Rao, A. Calcium Signaling in Lymphocytes. *Current Opinion in Immunology* **2008**, 20 (3), 250–258. <https://doi.org/10.1016/j.coi.2008.04.004>.
- (110) Yousefi, N.; Tufenkji, N. Probing the Interaction between Nanoparticles and Lipid Membranes by Quartz Crystal Microbalance with Dissipation Monitoring. *Front. Chem.* **2016**, 4. <https://doi.org/10.3389/fchem.2016.00046>.